UNIVERSITY OF CALIFORNIA SAN DIEGO

Development of A Luminal Esophageal Temperature Monitoring Device for Use During Treatment of Atrial Fibrillation

A Thesis submitted in partial satisfaction of the requirements

for the degree Master of Science

in

Engineering Sciences (Mechanical Engineering)

by

Scott Garner

Committee in charge:

Professor Frank E. Talke, Chair
Professor Renkun Chen
Professor Michael Tolley

2018

The Thesis of Scott Garner is approved, and is acceptable in quality and form for publication on microfilm and electronically.

_____

_____

_____

Chair

University of California San Diego

2018

TABLE OF CONTENTS

LIST OF FIGURES

LIST OF TABLES

ACKNOWLEDGMENTS

I would first like to thank Professor Talke for investing in me and giving me the opportunity to research this subject in his lab. I am grateful for his guidance and support throughout the time I have worked with him. His lessons, personally and professionally, will stay with me as I begin the next chapter of life and my career in engineering. In addition, I would like to thank Professor Tolley and Professor Chen who took interest in my work and helped guide me through several meaningful discussions. I also thank Dr. Feld and Dr. Savides whose medical expertise and suggestions for this work were invaluable.

I would also like to thank my fellow lab mates who have been very supportive and encouraging over the past year. I especially thank Karcher Morris, without whom my research would have been much more difficult. I am very appreciative of his guidance and mentorship through many aspects of my work. I also thank my fellow Jacobs Undergraduate Mentoring Program coordinators and staff for mentoring me in many ways and making my time at UC San Diego more enjoyable. Furthermore, I would like to acknowledge the Rady School of Management L2M team, Innovation for the Global Entrepreneur's technology accelerator, and the UCSD Office of Innovation and Commercialization for their help in progressing this research closer to having a real-world impact.

Finally, I would like to thank my family and friends for everything they have done to help set me up for success. It is with their help that I have made it to where I am today, and I will always be extremely grateful. I especially thank my best friend Kylie Saddler. She significantly helped our team with this project and has been constant source of love and support through the past two years of our graduate school experience and beyond.

ABSTRACT OF THE THESIS

Development of A Luminal Esophageal Temperature Monitoring Device for Use During Treatment of Atrial Fibrillation

by

Scott Garner

Master of Science in Engineering Sciences (Mechanical Engineering)

University of California San Diego, 2018

Professor Frank E. Talke, Chair

Luminal esophageal temperature monitoring is of high importance during catheter-based ablation procedures in the left atrium of the heart. An electrophysiologist's ability to reliably monitor significant temperature increase created by local ablative heat transfer is crucial to preventing thermal injury of the esophagus. The work presented here describes the initial development of a device intended to accurately measure temperature of the inner esophageal wall during treatment for atrial fibrillation. An experimental setup has been developed using porcine

esophageal and left atrial tissue and tests have been performed to better understand heat flow through the biomaterials in contact. To compliment ex vivo experiments, a numerical study using thermal finite element analysis has been implemented to investigate the temperature distribution across tissue layers as a function of tissue thickness, as well as heat source application time. Both the ex vivo study and finite element simulations aid in development of a practical prototype device for potential use during catheter ablation.

1. Introduction

1.1 Atrial Fibrillation and Methods of Treatment

Atrial fibrillation (AF or AFib) is one of the most common and severe types of arrhythmia, affecting millions of people worldwide [1,2]. Atrial fibrillation is caused by the generation of irregular electrical impulses in the atria which forces the heart to beat erratically [2]. These irregularities impede the heart's ability to effectively pump blood into the ventricles and thus to the rest of the body. This increases risk for a myriad of health issues such as heart-related death and stroke. Approximately one fifth of people who have a stroke also have AFib [2]. Figure 1 displays a labeled schematic of the human heart.

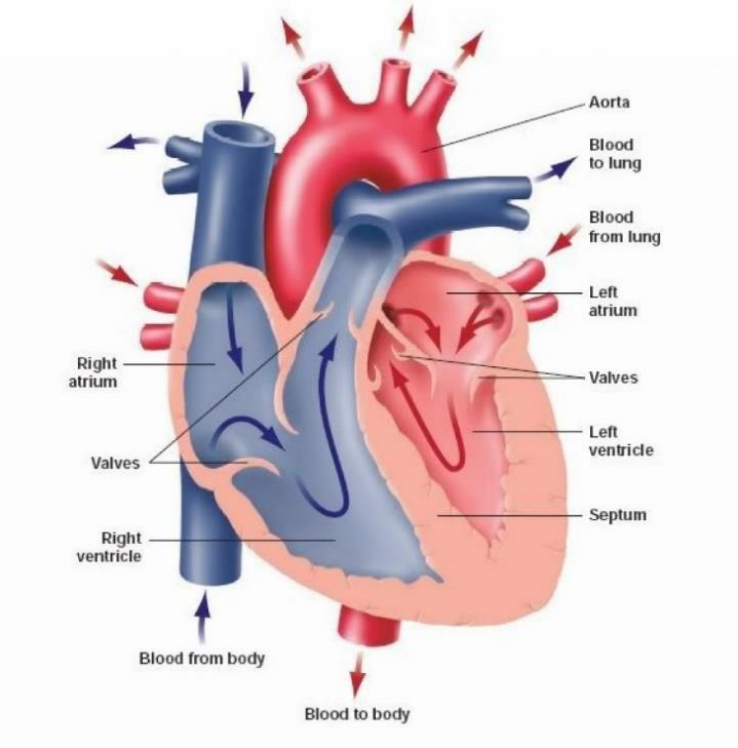

Figure 1: Labeled schematic of the human heart [3].

Treatment for rhythm control is frequently achieved using cardioversion and/or antiarrhythmic medication [1]. Recurrence rates after cardioversion therapy is predictably high at approximately 66%, but are significantly lower with the use of antiarrhythmic medication (approximately 33%). However, some long-term medication regiments can be harmful to the body. For example, Amiodarone is one commonly prescribed rhythm control medication with negative dose-dependent side effects on organs such as the lungs, liver, and thyroid [4]. Furthermore, antiarrhythmic medication can be expensive and create a financial burden on patients, especially those who are required to take them for many years of their life. Due to the drawbacks of these treatments, clinicians have sought out additional, non-pharmacological treatment options for AFib. More permanent solutions typically require surgery which has led to the development of a wide range of medical devices in this space. While some of the devices are created to increase the efficacy of the surgical procedure, others are specifically oriented for patient safety.

One increasingly common and curative form of treatment for AFib is catheter-based ablation. Catheter ablation has been used for decades to treat AFib [1,5], but over time has evolved significantly with respect to efficiency and safety, allowing the procedure to become widely accepted among the electrophysiology community. Catheter ablation is a minimally invasive surgery that begins with guiding a series of catheters into the left atrium of the heart via intracardiac echocardiography (ICE) [6] as shown in Figure 2.

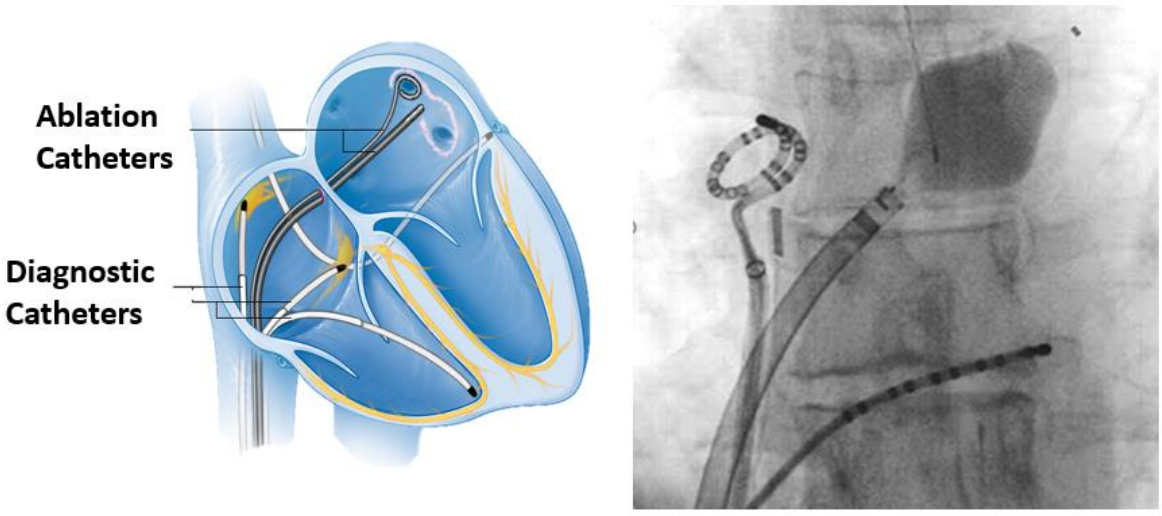

Figure 2: Catheters inserted into the left atrium via transseptal puncture prior to a catheter ablation procedure: schematic of catheters the left from the Mayo Clinic [7] (left) and actual photo under fluoroscopy from Reddy et al [6] (right).

Next an electroanatomic mapping procedure shows where normal and abnormal electrical activity occurs [1,8]. Figure 3 shows an electroanatomic mapping of the left atrium using the CARTO 3 system by Biosense Webster [8]. Regions of purple indicate areas of normal voltage and regions of red indicate areas of abnormal (unsafe) voltage [1,8]. The regions of red are predominant in the pulmonary veins because of ectopic foci that generate these electrical signals [1,5,8].

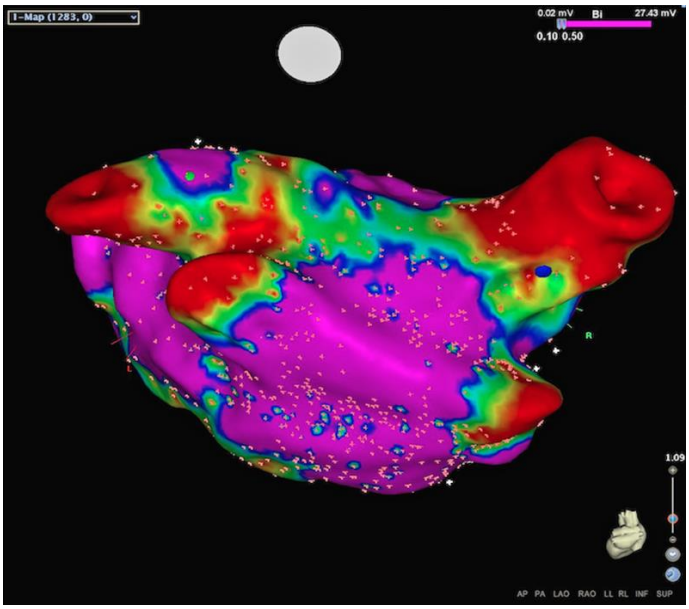

Figure 3: Voltage mapping of the left atrium using the CARTO 3 system by Biosense Webster [8].

An ablation catheter then delivers energy to tissue at the ostium of the four pulmonary veins. This is known as circumferential/segmental pulmonary vein isolation and is performed to create scar tissue that will block irregular signals from propagating through the rest of the heart [1]. The energy delivered to the atrial tissue is typically radiofrequency (RF) energy set to heat the tissue past a temperature where it is irreversibly damaged (~50 °C) [1,9]. Other forms of energy have also proven effective in ablating tissue, such as cryoenergy, which has complications mentioned in a later section of this paper. In 2016, there were approximately one million of these life-changing catheter ablation procedures performed worldwide, with close to one fourth of them taking place in the United States alone [1,2]. While substantial, the number of patients who receive catheter ablation only represent a small percentage (2.5%) of the total patient population diagnosed with AFib [10], as shown in Figure 4.

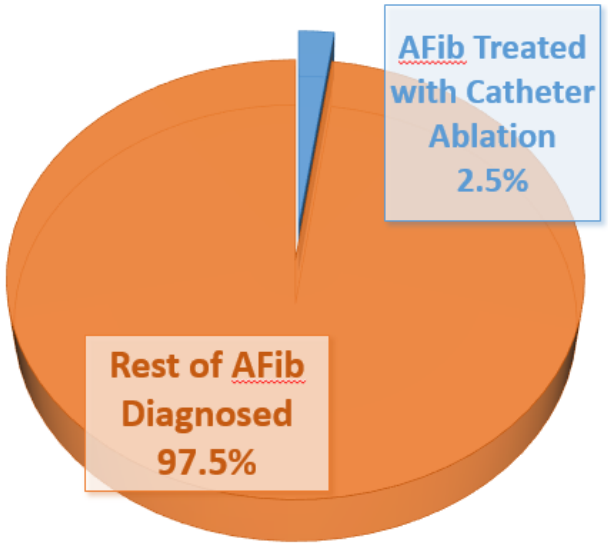

Figure 4: Pie chart showing the percentage of patients with diagnosed AFib who undergo catheter ablation. Information obtained from the 2016 Annual St. Jude Investor Presentation slides [10].

1.2 Thermal Injury to The Esophagus

One major risk associated with catheter ablation is thermal injury of the esophagus. The esophagus is a long tubular muscle that connects the pharynx to the stomach and facilitates movement of food and liquid to the digestive organs. Thermal injury may occur due to the proximity of the esophagus to the ablation site and local conductive heat transfer through the left atrium [1,9,11,12]. The medial portion of the esophagus is situated between the heart and the spinal column as shown in Figure 5. It can, however, move slightly and change its position which varies patient to patient. In up to 50% of cases, the esophagus is in direct contact with the left atrium during ablation [13].

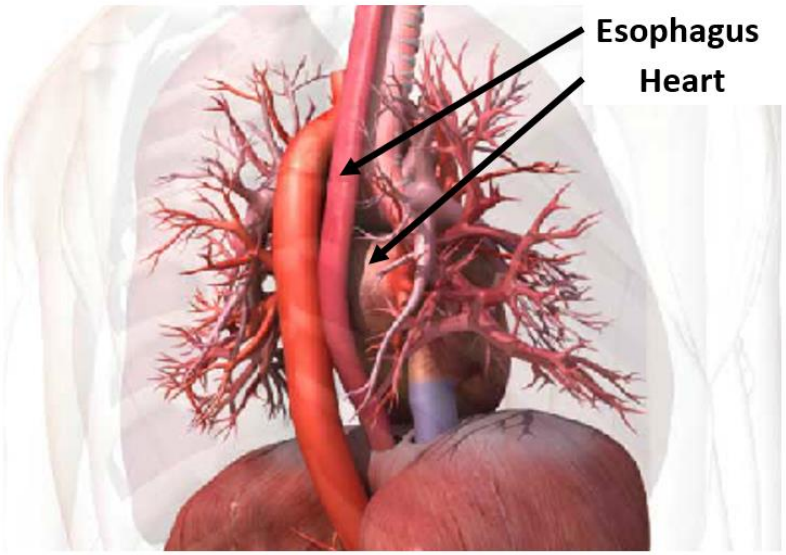

Figure 5: Anatomical relationship between the heart and the esophagus in the human body. Original picture obtained from HealthLine Newsletter [14].

The severity of injury varies because of the difficulty or inability for the electrophysiologist to reliably control several risk factors during the procedure. These include, but are not limited to, contact pressure between the catheter and left atrial wall, catheter orientation, catheter tip diameter, and duration of energy delivery [1,6,7,11].

In approximately 15% of patients whose esophagus is in close proximity to the ablation site, mild lesions or ulcers may form on the esophageal wall but are likely to heal [1]. In severe cases, atrio-esophageal fistulae develop from larger ulcerations, accounting for one of the most serious consequences of this treatment [1,6,7,9,11]. This complication is especially concerning because the fistulae may take a long period of time to form and the ensuing tissue necrosis is often diagnosed after it is too late to treat [15,16]. Figure 6 shows an example of an atrio-esophageal fistula and the opening created by the ablation catheter on the posterior wall of the left atrium [16]. In the photo on the left of Figure 6, “SVC” is the abbreviation for superior vena cava, and “IVC”

is the abbreviation for inferior vena cava. In the photo on the right, “LSPV” is the abbreviation for left superior pulmonary vein.

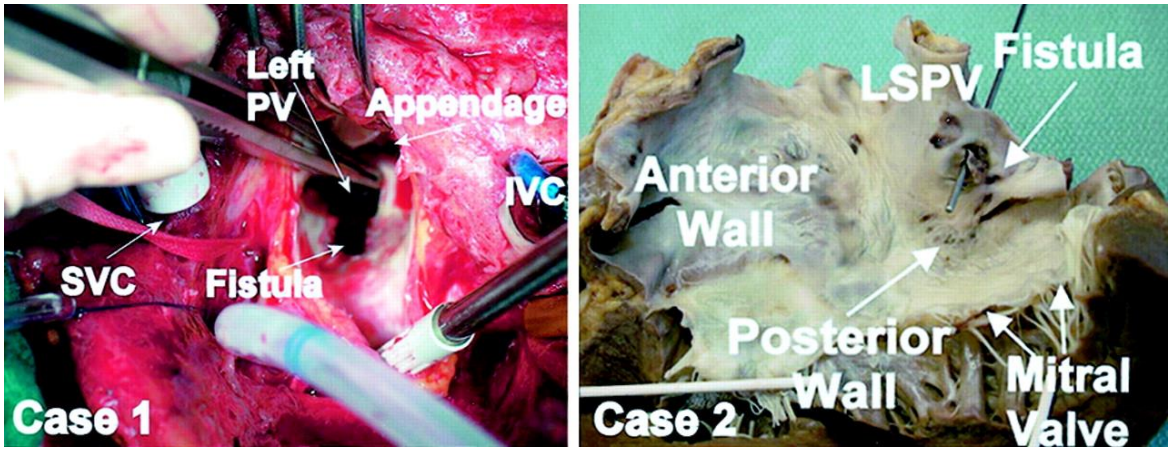

Figure 6: Photo obtained from Pappone et al [16] displaying an example of an atrio-esophageal fistula.

It is of high importance that the electrophysiologist performing the procedure can detect when the esophagus is in danger of being damaged by monitoring luminal esophageal temperature throughout the duration of the ablation and therefore knowing when to abort energy delivery when there is a critical increase in luminal esophageal temperature. It has been shown that a temperature of 40 °C is enough to initiate ulcer formation [17]. As ablation-based treatment methods become safer and more efficient, and with steady overall demand increasing for catheter-based treatments worldwide [1], there is a definitive need for further development of devices to protect the esophagus from injury. This is especially true for luminal esophageal temperature monitoring, which is now performed in almost all procedures [1,4,7].

1.3 Prior Work in Luminal Esophageal Temperature Monitoring

Singh et al [17] were first to show a decrease in esophageal injury when temperature probes were placed in the esophagus during ablation. Further, Perzanowski et al [18] describe how real-time monitoring of luminal esophageal temperature could accurately detect the onset of esophageal

heating, indicating to physicians when to cease energy delivery and let the esophagus return to its natural steady-state temperature before continuing with the procedure.

In a 2017 meta-analysis published in the Journal of Atrial Fibrillation, Koranne et al [17] describes how underestimation of intramural esophageal tissue is a major limitation of this monitoring, and that luminal esophageal temperature monitoring will overall remain the best strategy to detect heating of the esophagus. The authors illustrate the necessity and current lack of technology capable of accurate temperature monitoring and moving the esophagus away from the ablation site. It is also noted that luminal esophageal temperature measurements are necessary for other forms of energy delivery like cryoablation, which cools the tissue to low enough temperatures to "burn" and be irreversibly damaged.

1.4 Luminal Esophageal Temperature Monitoring and Esophageal Deviation Devices

To date, there are multiple FDA approved devices on the market designed to measure and monitor luminal esophageal temperature in real-time. Figure 7 displays two of these devices. The S-CATH by CIRCA Scientific [19] and SensiTherm by St. Jude Medical [20] both use a multiplicity of temperature sensors to record temperature in the esophagus during ablation. The SensiTherm device consists of five thermocouples linearly spaced along a flexible and insulated tube [20]. The S-CATH is a two-dimensional array of twelve temperature sensors placed along a thin flexible tube that relaxes to an "S" shape after a long insertion piece is removed from its lumen [19].

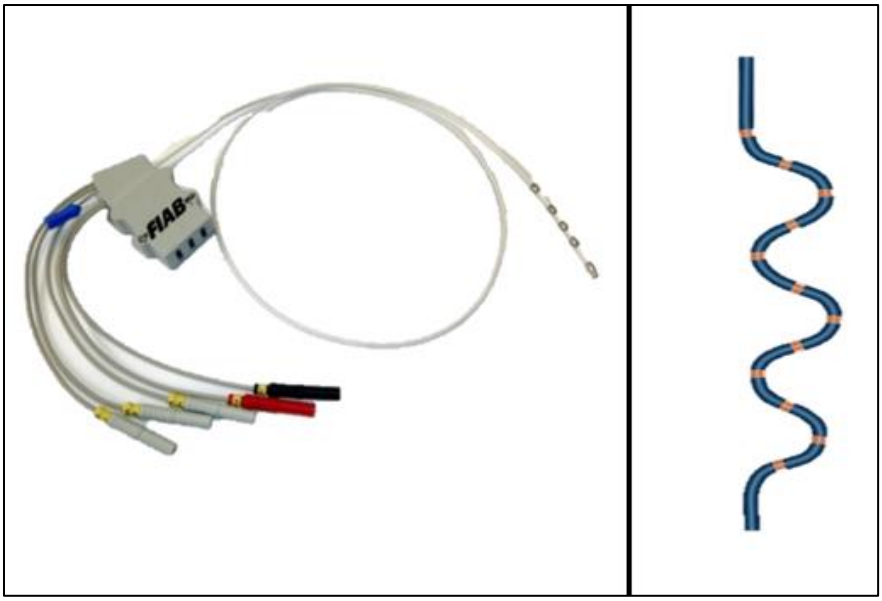

Figure 7: Two commercially available luminal esophageal temperature monitoring devices: SensiTherm by St. Jude Medical [20] (left) and S-CATH by CIRCA Scientific [19] (right).

Another category of devices intended to protect the esophagus is deviation. It has been recommended that deflecting the esophagus approximately 2-3 centimeters away from the ablation site is sufficient to prevent esophageal damage [9,17]. Two common and commercially available devices that deviate the esophagus are the Esophageal Retractor by EsoSure [21] and DV8 by Manual Surgical Sciences [22]. Both are shown in Figure 8. The EsoSure Esophageal Retractor uses a shape-memory alloy (nitinol) wire that is trained to activate when it reaches core body temperature (~37 ℃). The nitinol begins straightened and transitions into its deflected state after insertion into the esophagus [21]. The DV8 device uses a balloon located at the distal end of a flexible rod. When inflated, the balloon creates a shape that deflects the esophagus [22].

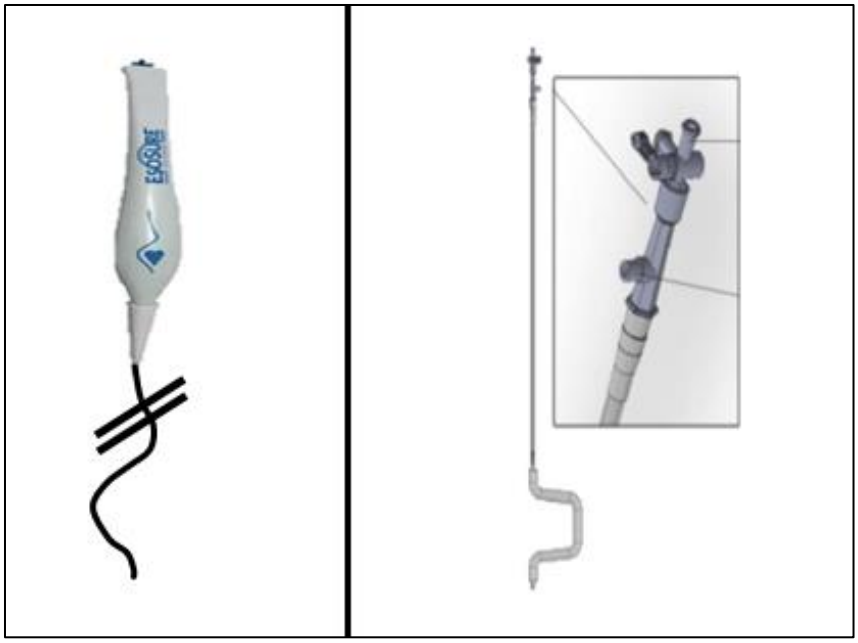

Figure 8: Two commercially available esophageal deviation devices: DV8 Balloon by Manual Surgical Science [22] (left) and EsoSure Retractor by EsoSure [21] (right).

While deflection does protect the esophagus, it is typically not performed unless necessary [1,13]. It is the temperature measurement devices that alert the electrophysiologist when it is necessary to use a deviation device, usually after only a 1-2 ℃ rise in luminal esophageal temperature is recorded [1,7,9,11]. Before the widespread use of commercially available devices, a more traditional approach was required for diverting the esophagus away from the ablation site. When the 1-2 ℃ rise was detected, the electrophysiologist would stop ablation and require a gastroenterologist to move the esophagus with a steerable endoscope before the electrophysiologist could continue ablating the left atrium [13]. This approach is very cumbersome and illustrates how the inefficiencies create problems that affect not only the patients, but also the doctors and the hospital. In fact, in many cases the gastroenterologist may not be available if he/she is working on other cases. This method is sometimes still practiced in hospitals, but less frequent due to the increase in available deflection technology.

Inserting multiple devices in the esophagus may also create difficulties in maneuvering each device individually without obstructing the other. In the case of the S-CATH by CIRCA Scientific, it is more difficult to manipulate after its insertion tab is removed. Additionally, the number of radiopaque markers found on both types of devices could potentially interfere with guiding the mapping and ablation catheters into the correct position under fluoroscopy [6,11]. These devices are complex and may need special training to use properly and safely.

1.5 Thesis Overview

There is currently a gap in the technology for a device that is capable of both luminal esophageal temperature monitoring and esophageal deviation simultaneously. This would eliminate the need for a second physician and/or a second device used to accomplish the task of protecting the esophagus, saving time and money for most or all parties involved. For example, the patient may have reduced procedure time and reduced insurance-related costs in the case that multiple devices and/or multiple physicians would have been used in their specific case. Hospitals could potentially perform more catheter ablation procedures annually and would not need to purchase multiple types of devices. The electrophysiologist would need less training on multiple devices and would not need to stop their workflow for potential gastroenterologist intervention.

This paper discusses the preliminary development of such a device that is capable of both luminal esophageal temperature monitoring and esophageal deflection. The intention is primarily to investigate how the proposed device could overcome limitations/unknowns of current technology and implementation into a biocompatible device using rapid prototyping. One significant unknown is the adequate number of sensors needed to accurately and confidently gauge an increase in luminal esophageal temperature near the ablation site. Ablation catheters are very efficient in delivering energy in a small localized area [1,5,17]. Therefore, it is necessary that a

sufficient quantity of sensors be placed close enough together so they can detect any dangerous temperature rise in the scenario that heat is transferred between two adjacent sensors. Another obstacle for luminal esophageal temperature monitoring devices is ensuring contact between the sensors and the luminal esophageal wall throughout the entire procedure. Because luminal esophageal temperature monitoring is, at best, an underestimate of outer esophageal wall heating [7,17], it is crucial that the sensors stay in contact with the inner wall for optimal measurements.

A better understanding of the heat transfer through the left atrium and esophagus is vital to better understanding these unknowns. In a pilot study by Leite et al [23], in vivo luminal esophageal temperature was monitored in a series of human studies. This was done with a temperature sensor located at the distal end of a deflectable catheter. Intracardiac echocardiography of the esophagus was used as an indication of when the catheter may be deflected toward the ablation site when the esophagus was visualized to be adjacent to a targeted site in the left atrium. Energy delivery was aborted when an increase of 2 ℃ was recorded by the temperature sensor, which occurred one or several times in all patients involved in the study. When an ablation yielded an increase of 2 ℃, the maximum luminal esophageal temperature occurred an average of 11.8 s after ablation. It is noted that lining up the single sensor with the ablation site is difficult and tedious under fluoroscopy. The authors also stress the importance of sensors being placed as close as possible to the ablation site; otherwise, recorded temperature rise may be much to slow to detect when to abort unsafe energy delivery. Similar studies have been performed with balloon-like catheters to minimize distance from temperature sensors to the ablation site [17,23]. Although this ensures contact between the sensor and luminal esophageal wall, thus increasing the accuracy of the reading, it may introduce risk of pressing the esophagus into the ablation site and overall increasing the risk of damage. In two different computational studies, Fasano et al [11] and

Perez et al [24] show that the use of common esophageal temperature probes (ETPs) is safe to implement with respect to risk of electrical conduction when exposed to the RF emitting catheter. This is also known as the “RF antenna effect” [24]. The studies also show that the location in which RF energy coverts to heat is very close to the surface in which the ablation occurs. Perez et al discuss how temperature in the tissue layers likely increases quickly due to thermal conduction without any electrical interaction.

In the following sections, an experimental study and a numerical study of the temperature rise in the esophagus from ablation are discussed. These studies were performed to better understand the conductive heat transfer from the ablation catheter to the luminal esophageal wall. The results are also used to infer how many temperature sensors may be sufficient and how far apart the sensors will be placed on the proposed device. The information is organized such that the methods, results, and discussion for each study are grouped together. This grouping makes it more convenient for the reader to focus on one study at a time. An existing physical structure/design that is described in a later section will act as the main platform for which these luminal esophageal temperature measurement capabilities are incorporated. Commercialization aspects for the proposed device are also considered; potential reimbursement and regulatory options are compared for how each will affect the design process and how they may drive decisions to bring the device to market.

2. Ex Vivo Study

2.1 Experimental Setup and Methods

Heat transferred through layers of tissue via conduction during catheter ablation needs to be better understood. Ex vivo tests were first used to aid this understanding. Tests were set up to mimic catheter ablation in the left atrium and record the associated local heat transfer to the

esophagus via temperature sensor data. Figure 9 shows the anatomical relationship between the left atrium and the esophagus in the sagittal plane of a cadaver [25]. The sagittal plane cut shows the contact between the left atrium and the esophagus. This direct contact is a worst case-scenario for the esophagus and was implemented in mimicking ablation in the ex vivo studies.

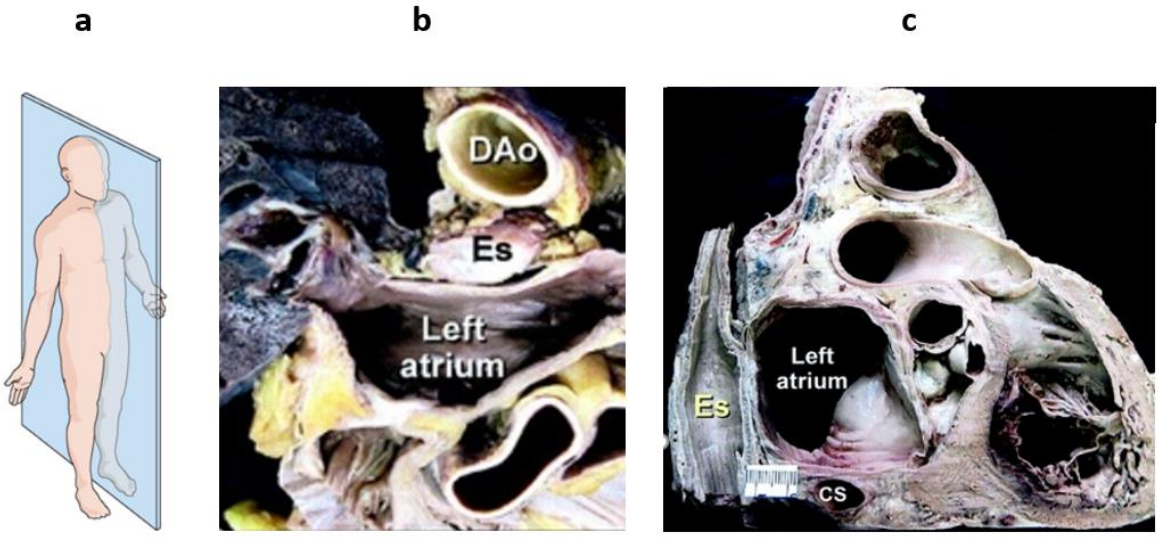

Figure 9: Anatomical relationship between the left atrium and the esophagus from Quintana et al [25]: a) plane of sagittal cut, b) topside view of esophagus and left atrium before sagittal cut, and c) orthogonal view of esophagus and left atrium after the sagittal cut.

Samples of porcine esophageal and left atrial tissue were excised to best match their area of contact in the human body. Quintana et al [25] show that the average area of contact between the left atrium and the esophagus is 8 square centimeters (4 centimeters by 2 centimeters). Figure 10 shows the front and back sides of the two sections of tissue that were cut to approximately match these dimensions. Approximately 2 centimeters of extra tissue was left on each end of the tissue samples for clamping them together. The porcine heart and esophagus were harvested and tested within 2 days.

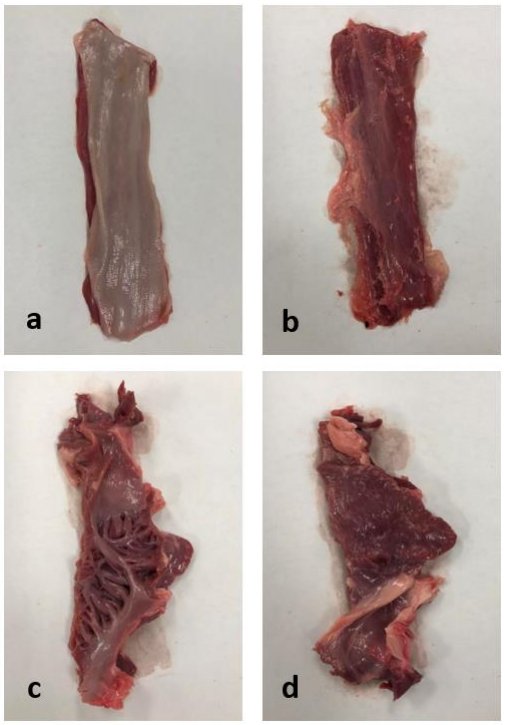

Figure 10: Excised porcine tissue for ex vivo study: a) interior esophageal tissue, b) exterior esophageal tissue, c) interior left atrial tissue, d) exterior left atrial tissue.

A constant-temperature metallic heat source at 55 ℃ was used in place of an RF ablation catheter. This temperature was chosen because it is a common maximum temperature recorded by temperature sensors located at the tip of RF ablation catheters at the termination of a 30 W, 60s ablation [26,27]. Using this temperature bounds the problem in worst-case type scenario. The temperature load curve recorded at the catheter-endocardium interface in an actual procedure is not constant and instead follows a nonlinear curve with asymptotic behavior, shown later in this section. The cylindrical heat source had a diameter of five millimeters and is displayed in Figure 11.

Figure 11: Cylindrical heat source used in ex vivo studies to mimic catheter ablation.

The temperature sensors chosen for the ex vivo studies were commercially available negative temperature coefficient (NTC) thermistors. NTC thermistors decrease in resistance when subjected to an increase in temperature (and vice versa) and are commonly used for temperature monitoring in medical devices for their high sensitivity and quick response time [28]. Positive temperature coefficient (PTC) thermistors increase in resistance when exposed to an increase in temperature and have a slower response time. This slower response makes them less desired for this application. The specific 10 kΩ thermistors chosen, shown in Figure 12, are manufactured with the intent of fitting into open channels in catheter assemblies and thus are very small. This benefits the design of the luminal esophageal temperature measurement device because there can be a higher density of sensors on the device near the ablation site.

Figure 12: Commercially available 10 kΩ NTC thermistors used in ex vivo studies.

A temperature reading from a thermistor was achieved by converting its resistance value using a temperature versus resistance calibration curve. Calibration curve functions and/or temperature and associated resistance data are typically given by the thermistor manufacturer. Because thermistors are temperature-dependent resistors, they are easily implemented into a voltage divider circuit to calculate its resistance. Figure 13 shows a typical voltage divider circuit, in which resistance R_1 is a known, user-defined value (4.52 kΩ) and R_2 is the unknown thermistor resistance. A known voltage V_{in} (5 V) is applied to the circuit and a voltage V_{out} is read across the unknown thermistor. Equation 1 displays the relationship between the two resistances and voltage values. Equation 2 shows Equation 1 solved in terms of the unknown resistance R_2.

$$\boldsymbol{V_{out} = V_{in}\left(\frac{R_2}{R_1+R_2}\right)} \qquad (1)$$

$$\boldsymbol{R_2 = \frac{R_1}{\left(\frac{V_{in}}{V_{out}} - 1\right)}} \qquad (2)$$

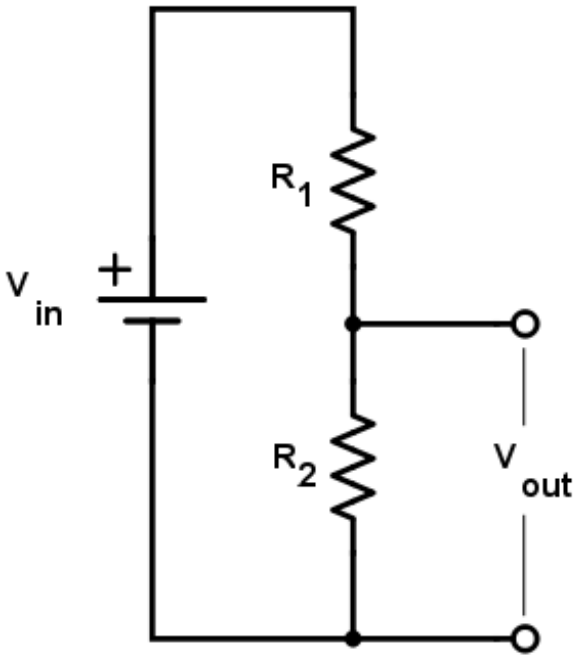

Figure 13: Schematic of voltage divider circuit.

Figure 14 shows the wiring for multiple thermistors using a single breadboard. A microcontroller assisted by an analog to digital converter was used to read voltage signals across thermistors. The microcontroller was plugged into a laptop with commercially available MATLAB software. MATLAB communicates to the microcontroller to discretize analog values from a range of analog pins and converts them to the output voltage, V_{out}.

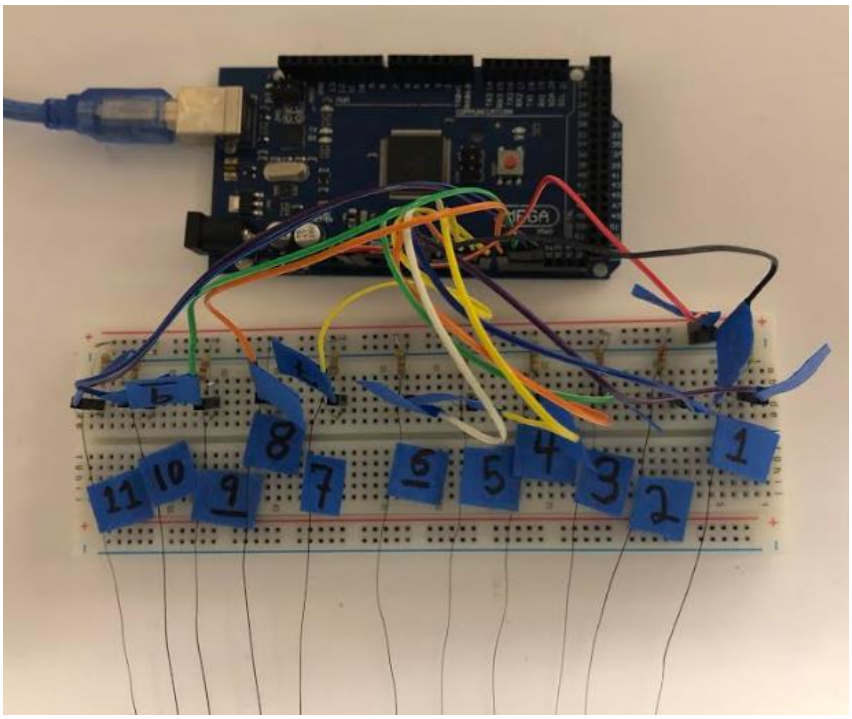

Figure 14: Voltage divider circuits created for each thermistor on a single breadboard. Jumper wires connect the circuit to a microcontroller with an adapter for connecting to a laptop computer.

Special care was taken to ensure consistent connectivity of all sensors. A calibration curve was created for each thermistor to avoid any error in resistance from the manufacturer's specified value. To do this, resistance values were taken for each thermistor at multiple known temperatures. These known temperatures were verified by a standard mercury thermometer suspended in a beaker of water on a temperature controlled hot plate. Next, a best fit curve was calculated for each set of temperature versus resistance data for each thermistor. These curves yield the expected nonlinear behavior of NTC thermistors. One of the calibration curves is shown in Figure 15. MATLAB then takes the output voltage and calculates the temperature reading in real time using the calibration curve function at a sampling rate of 5 Hz.

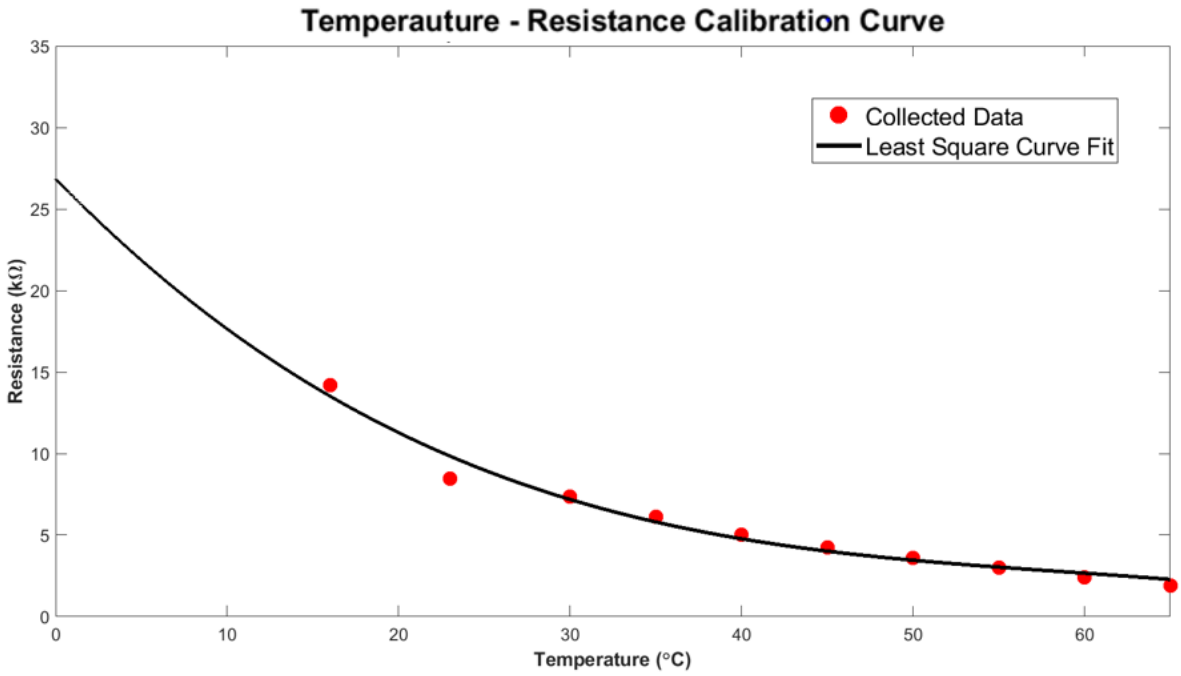

Figure 15: Resistance versus temperature calibration curve created for a single thermistor.

Two different sensor arrays were fabricated and clamped together with the two biomaterials in direct contact. Figure 16 displays the two different arrays of temperature sensors, each numbered for data collection described later in this section. The array of sensors with 6 thermistors is called Sensor Array #1and the array with 11 thermistors is called Sensor Array #2. Sensor Array #1 contains sensors with equal spacing of 10 millimeters between each. Sensor Array #2 contains sensors with a spacing of 5 millimeters between each, making both sets the same length. The thermistors were adhered onto a 2-millimeter thick silicone layer and record temperature rises on the luminal esophageal tissue from the heat source applied to the left atrial tissue.

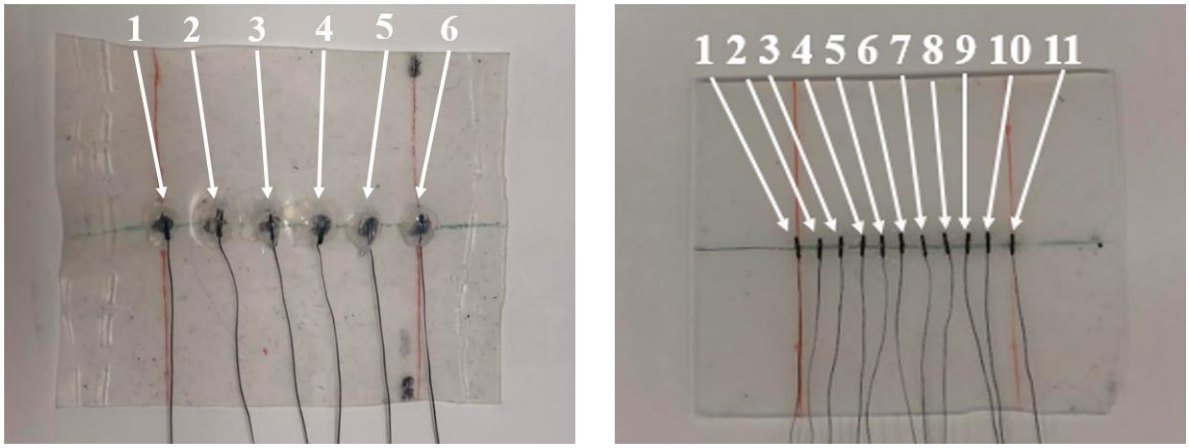

Figure 16: Thin layer of silicone with adhered temperature sensors used to collect real-time temperature data during ex vivo studies: 6-sensor array (left) and 11-sensor array (right).

The clamped tissues and silicone were placed on a perforated metal test stand with 3D Printed PLA supports to elevate the apparatus off the base. The silicone was clamped such that the sensors were in direct contact with the luminal esophageal tissue. Figure 17 shows both the schematic and actual setup prior to beginning any tests.

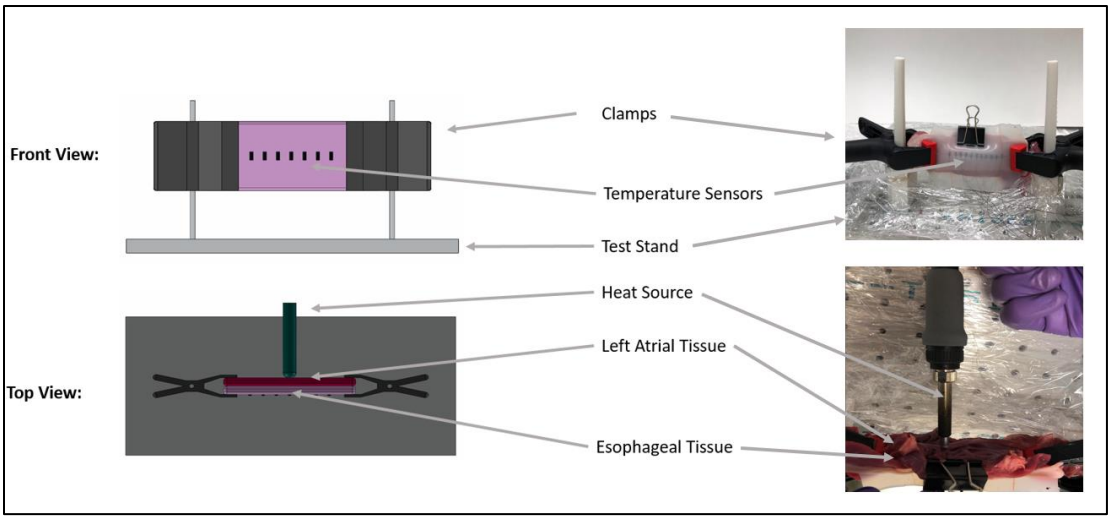

Figure 17: Experimental setup for ex vivo studies: schematic of the experimental setup (left) and actual setup (right).

The experimental procedure was as follows for Sensor Array #1:

- **Step 1.** Time = 0 s: Start recording temperature data.
- **Step 2.** Time = 30 s: Apply heat source to atrial tissue in line with sensor #3.
- **Step 3.** Time = 90 s: Remove heat source from atrial tissue.
- **Step 4.** Stop recording data once all sensors read ~25 °C.
- **Step 5.** Let tissue/sensors cool to steady-state for 10 minutes.
- **Step 6.** Repeat steps 1-5 behind sensors #5 and #4.

The experimental procedure was as follows for Sensor Array #2:

- **Step 1.** Time = 0 s: Start recording temperature data.
- **Step 2.** Time = 30 s: Apply heat source to atrial tissue in line with sensor #6.
- **Step 3.** Time = 90 s: Remove heat source from atrial tissue.
- **Step 4.** Stop recording data once all sensors read ~25 °C.
- **Step 5.** Let tissue/sensors cool to steady-state for 10 minutes.
- **Step 6.** Repeat steps 1-5 behind sensors #3 and #9.

An additional test was also performed with Sensor Array #2 to investigate the response from the sensors when a thin layer of Polydimethylsiloxane (PDMS) silicone placed between the sensors the esophageal wall is present. This was to simulate a thin biocompatible layer that may be present on the device between the sensors and the luminal esophageal wall. Figure 18 shows the 2-millimeter-thick layer of PDMS used as this barrier. The same procedure was followed by applying heat behind sensor #6 for 60 s and recording the response.

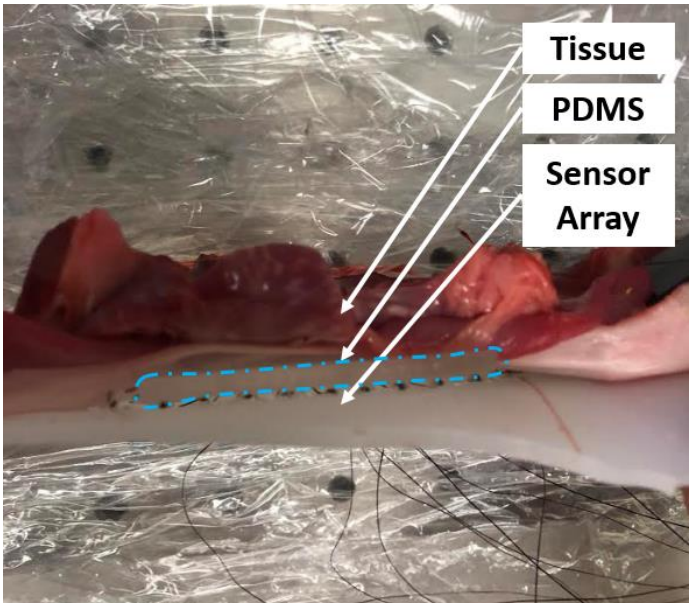

Figure 18: A thin layer of PDMS silicone (outlined in blue) inserted between the sensors and esophageal tissue.

2.2 Ex Vivo Study Results

Temperature data was plotted for each sensor array. The three tests conducted using Sensor Array #1 according to the procedure above are called tests A1, A2, and A3, respectively. The four tests conducted using Sensor Array #2 according to the procedure above are called tests B1, B2, B3, and B4, respectively.

A similar sensor response pattern is noticed in tests A1-A3. Test A1 shows that sensor #3 is the only sensor to record a significant increase in temperature. In test A2, sensor #5 is the only sensor that records significant increase in temperature. Last, Test A3 shows that sensor #4 is the only sensor that records significant increase in temperature. The maximum temperatures recorded for these three tests were 30.9 ℃, 31.64 ℃, and 33.2 ℃, respectively. The time elapsed for each sensor reading to increase by 2 ℃ was 21.5s, 17.5s, and 19.5s, respectively. The temperature versus time response from these tests are plotted and shown in Figures 19, 20, and 21, respectively.

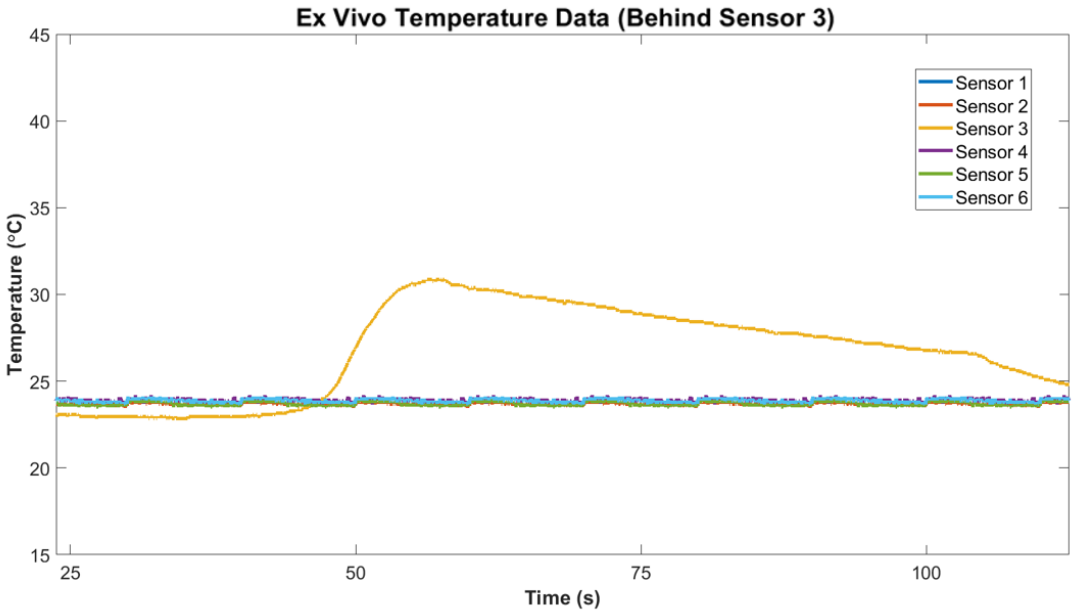

Figure 19: Time versus temperature sensor response data for test A1.

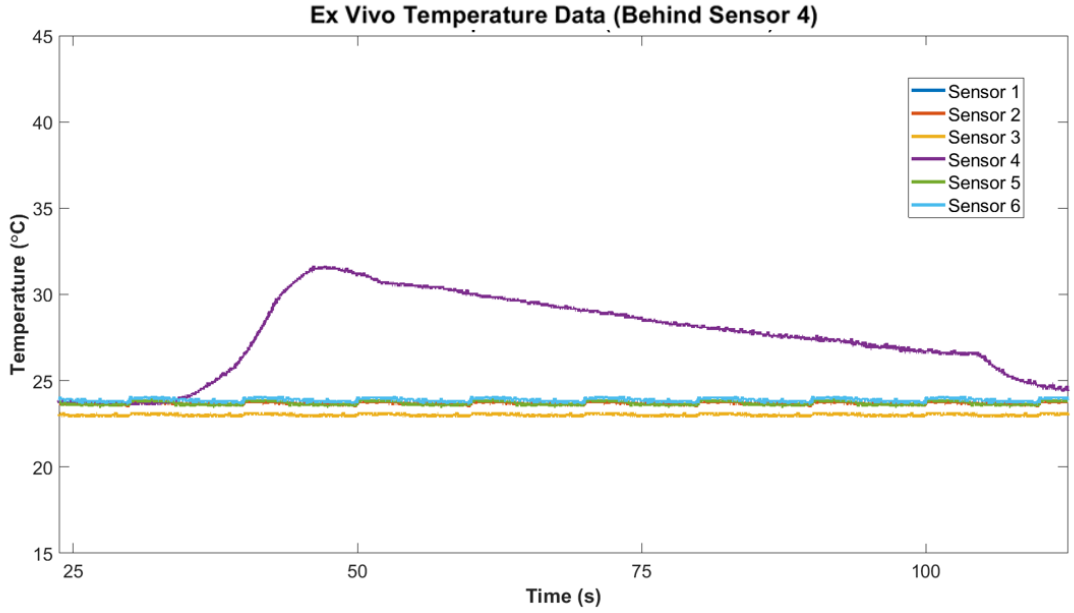

Figure 20: Time versus temperature sensor response data for test A2.

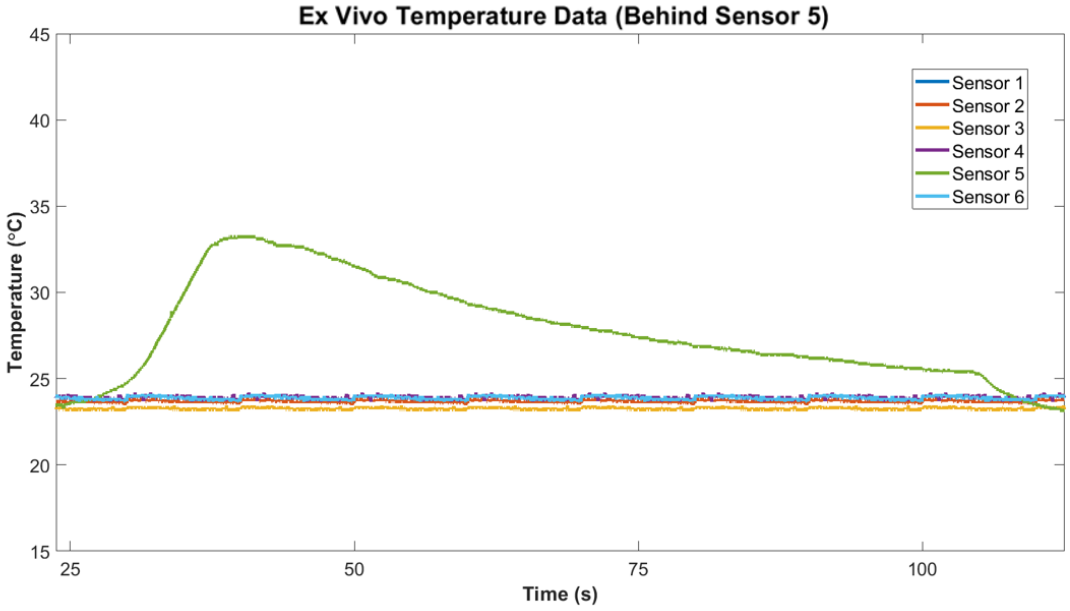

Figure 21: Time versus temperature sensor response data for test A3.

Tests using Sensor Array #2 show a different sensor response. Although the fourth test was only run on the second array, the implications of the result can be applied to the first array. Tests B1-B4 show a temperature increase recorded in multiple sensors. Applying heat in line with a specific sensor was more difficult with 11 sensors in comparison to 6 sensors due to their close spacing. Test B1 shows that sensor #5 sees the highest increase in temperature at 34.5 ℃. The next closest sensor affected is sensor #6, followed by sensors #4 and #7, respectively. A similar result is shown in test B2 where sensor #4 shows the largest increase at 33.1 ℃, followed by sensors #3, #5 and #2, respectively. Test B2 shows an attenuated response from affected sensors #10, #11, #9, and #8. The maximum temperature achieved for this test was by sensor #10 at 27.3 ℃. Test B4, using the extra silicone layer between the sensors and the esophageal tissue, shows much smaller temperature increase with the maximum occurring at sensor #6 at 25.7 ℃. The temperature versus

time response from these four tests are plotted and shown in Figures 22, 23, 24, and 25, respectively. The maximum temperatures and response times are tabulated in Table 1.

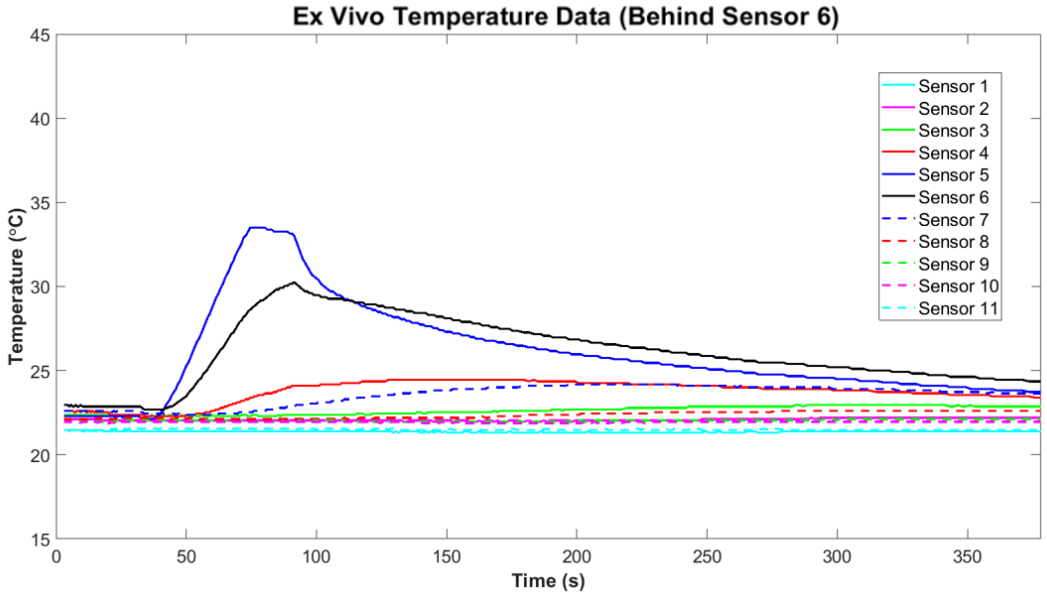

Figure 22: Time versus temperature sensor response data for test B1.

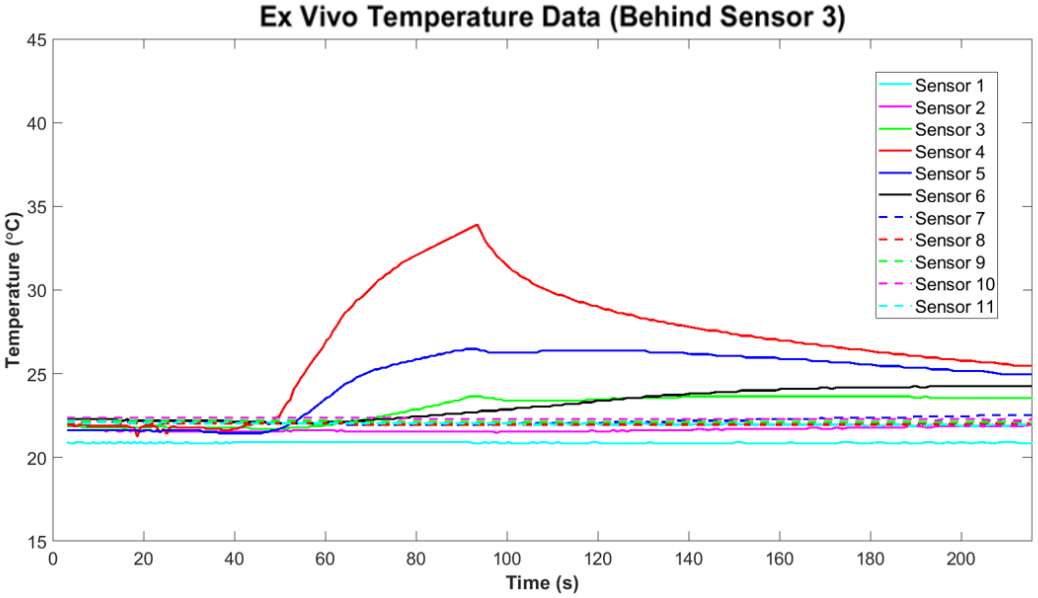

Figure 23: Time versus temperature sensor response data for test B2.

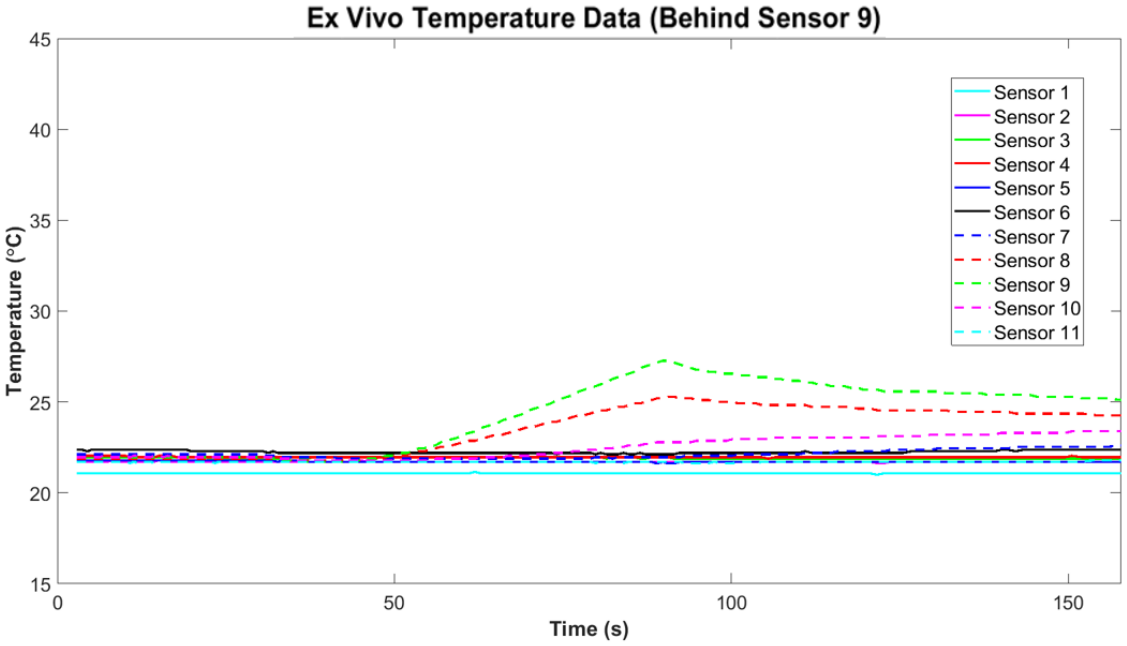

Figure 24: Time versus temperature sensor response data for test B3.

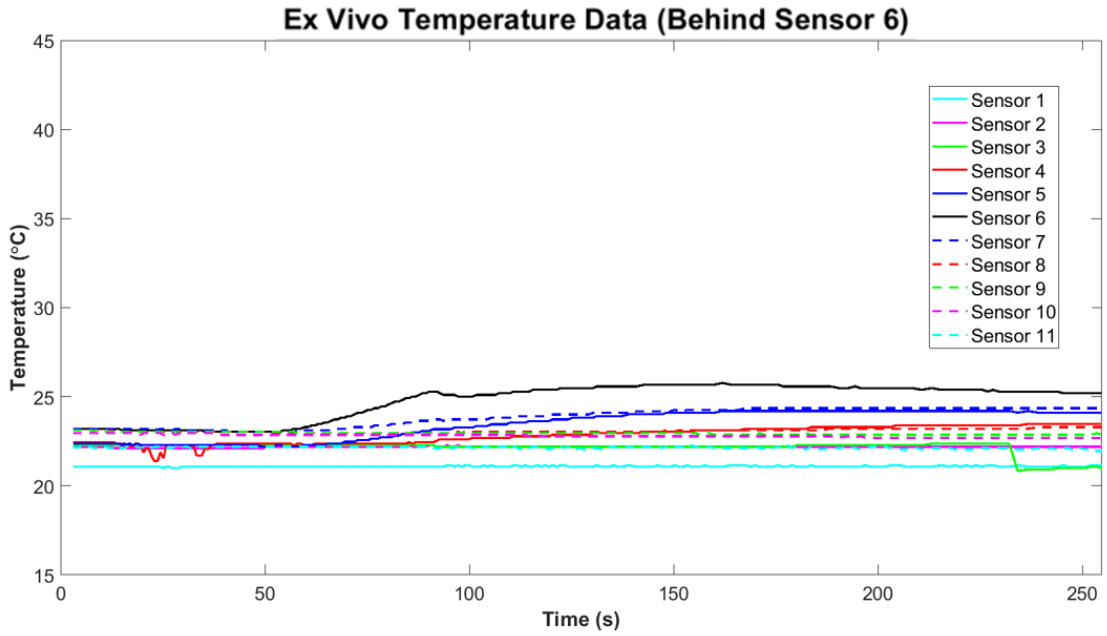

Figure 25: Time versus temperature sensor response data for test B4.

Table 1: Temperature sensor data for Array #2.

	Maximum Temperature (°C)	Sensor at Maximum Temperature	Time Elapsed for +2 °C Increase
Test B1	34.5	5	13.7
Test B2	27.3	10	19.0
Test B3	33.1	4	15.7
Test B4	25.7	6	28.3

3D surface plots of the temperature rise and fall were created in MATLAB using the time and spatial dependent temperature data from Tests B1-B4. These were not created for the results from Tests A1-A3 as they would not reveal useful information in the spatial direction since only one sensor read a significant increase at a time. The surface plots help visualize which area of the tissue samples were affected the most by the heat source and at what time. Temperature contour plots of the sensor readings were then created from the surface plots. The contours help to visualize rise time and sensed temperature gradients over time and space. Figures 26, 27, 28, and 29 show the surface and contour plots associated with the temperature data for tests B1-B4, respectively.

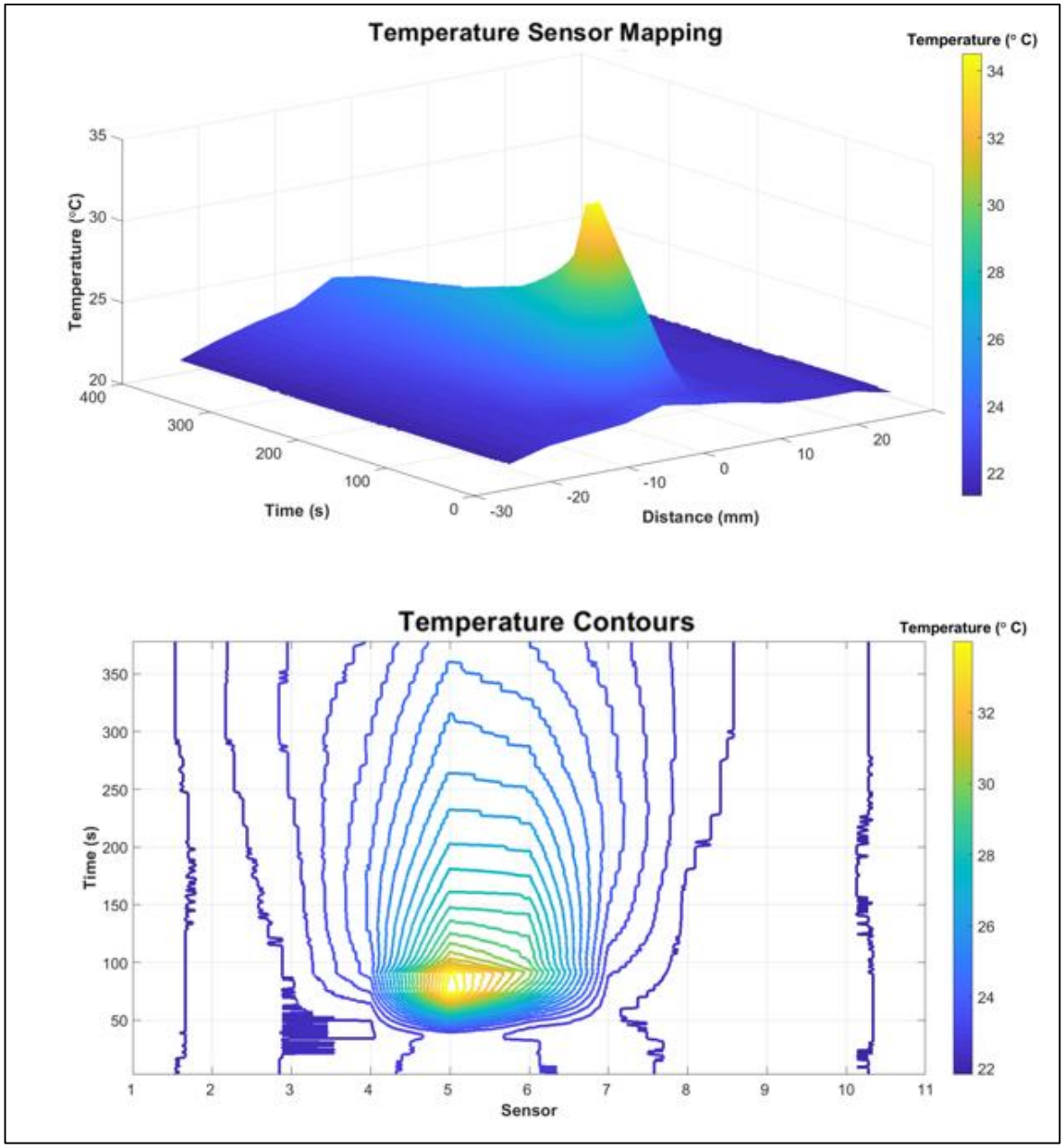

Figure 26: 3D surface and contour plots of temperature sensor data as a function of time and space for test B1.

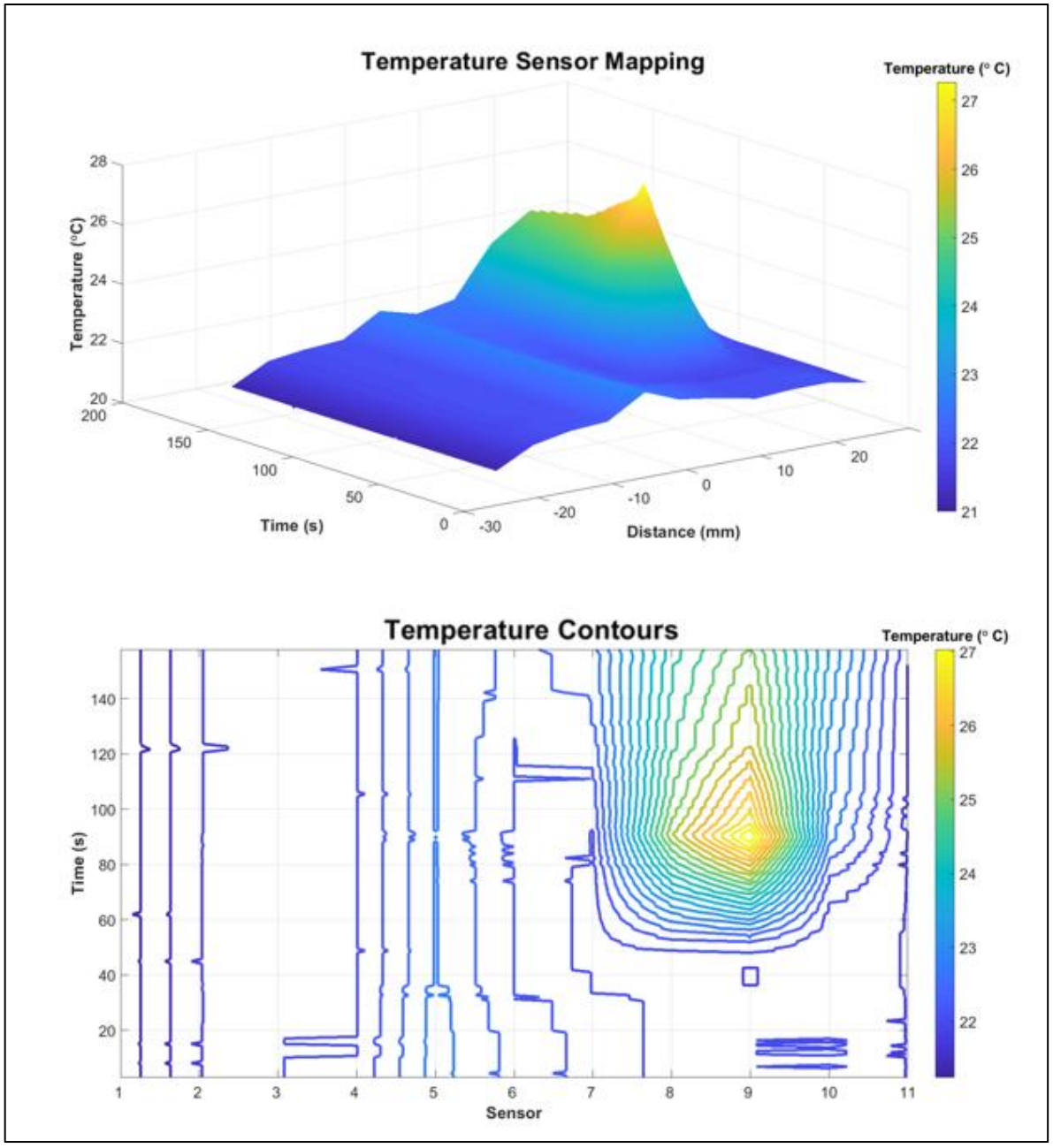

Figure 27: 3D surface and contour plots of temperature sensor data as a function of time and space for test B2.

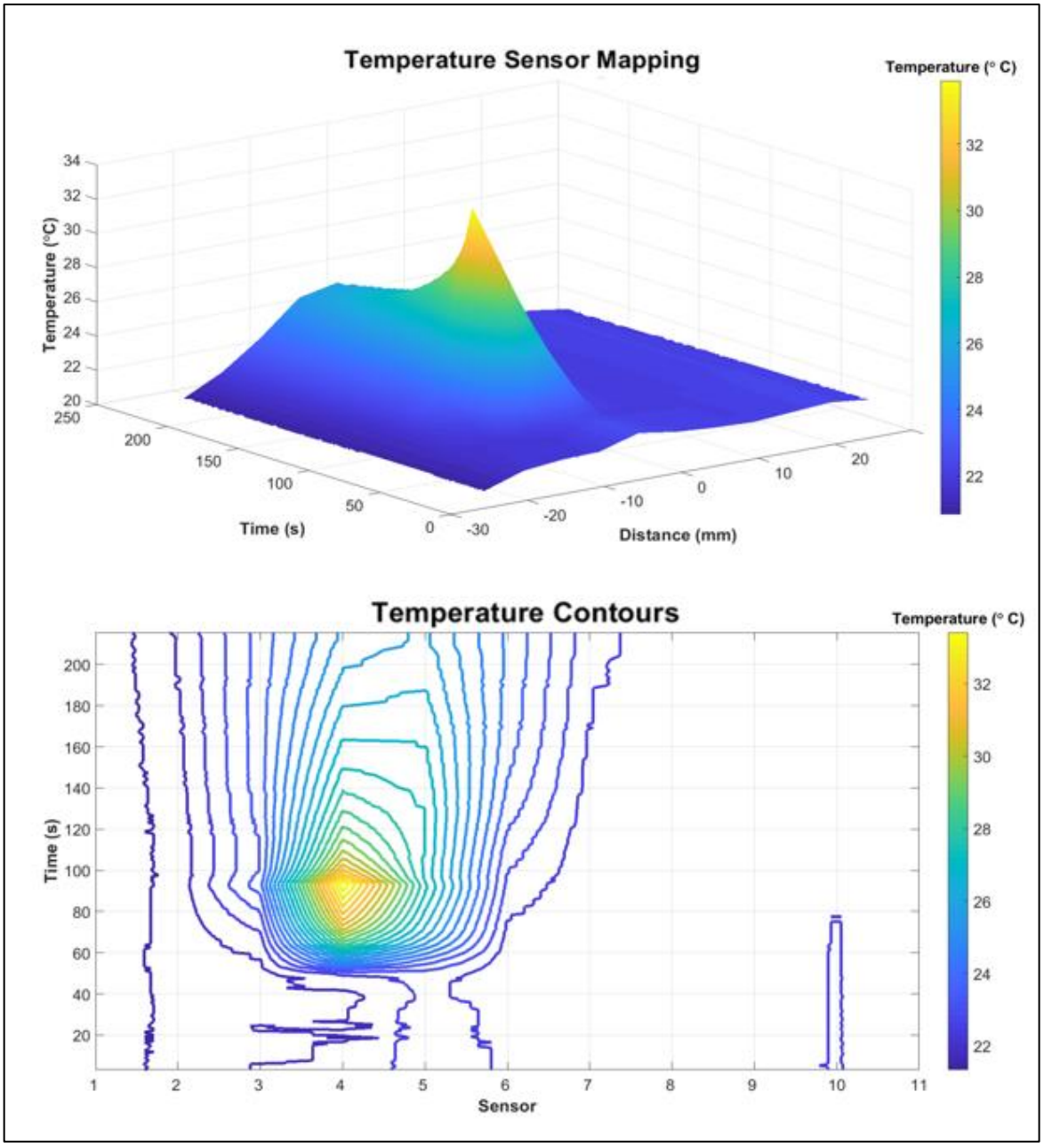

Figure 28: 3D surface and contour plots of temperature sensor data as a function of time and space for test B3.

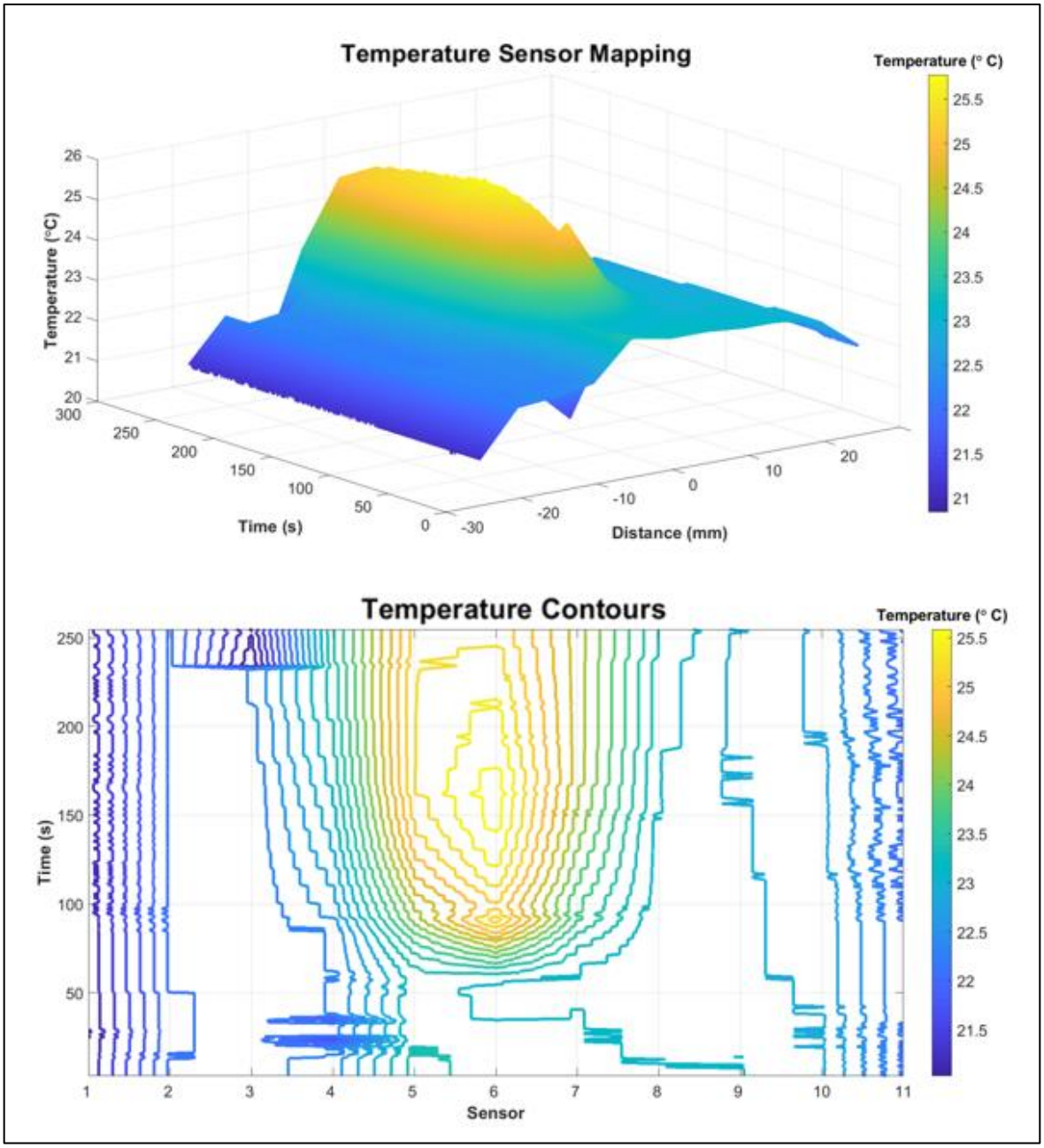

Figure 29: 3D surface and contour plots of temperature sensor data as a function of time and space for test B4.

2.3 Discussion of Experimental Results

Ex vivo studies show valuable results for appropriate sensor placement/spacing in the device. When using Sensor Array #1, only a single sensor could read a substantial temperature increase for each of the three tests. When using Sensor Array #2, multiple sensors could read a temperature difference for each of the four tests. This makes sense since the spacing of thermistors in Array #2 is half of that for Array #1. It was much more difficult to apply the heat source in line with a specific sensor at the left atrial wall during tests with Array #2. This is reflected in Table 1 where the location of the sensor detecting the highest temperature was not the sensor expected (see experimental procedure). In fact, test B2 shows that the heat source was likely applied along the centerline between sensors #10 and #11. This explains why the maximum temperature for these two sensors are both lower than the maximum seen in test B1 and test B3 but much higher than their other adjacent sensors.

The maximum temperatures from tests A1-A3 are overall lower than tests B1-B4. The time taken for the sensor to increase fastest by +2 ℃ was also higher for Array #1, indicating that there may have been less contact pressure used in comparison to Array #2. It makes sense that multiple sensors from array #2 would see an increase in temperature since the heat source had the same diameter as the spacing between each. This was shown to be helpful since the location the heat source was intended to be applied was different from the location it was applied for the first three tests. Thus, these tests reveal that it may be important to place the sensors with a spacing closer to or less than the diameter of the heat source to ensure a temperature rise in luminal esophageal temperature is captured by at least one sensor. In test B4, the shielding PDMS layer has an approximate thermal conductivity of 0.5 $\frac{W}{m*K}$ which acts as an additional thermal barrier between

the esophageal wall and the sensors. This explains why there is a lesser amount heat being transferred to the sensors and where a lower maximum temperature is seen in sensor #6.

Surface and contour plots of the recorded temperature create a thermal "map" of how the temperature is distributed at the luminal esophageal wall over time. Tests B1 and B3 show a similar surface profiles in which the rise time for the sensor achieving the maximum temperature is similar. In their corresponding contour plots, it is apparent which sensors experience a faster decline in temperature than others. For example, Figure 28 shows that the gradient of temperature for sensor #3 is much steeper than sensor #5. This shows more accurately where the heat source was applied, which in this case was mostly over sensor #6, but closer to sensor #5. Tests B2 and B4 show a slower rise time in comparison to Tests B1 and B3. Further, plots for Test B4 show how the heat is applied more uniformly to the tissue based on the wider profile and gradients in Figure 29. This makes sense due to the shielding PDMS layer between the sensors and the esophageal tissue. As the heat is transferred from the heat source through more material layers, the heat is spread more evenly which yield lower temperatures recorded at each sensor.

In tests where the heat source was applied between sensors (rather than on a single sensor), it is useful to interpolate what the maximum temperature is between them. An example of this interpolation is shown in Figure 30 in which a Lagrangian polynomial is fitted to the sensor data from test B1. The key points used for this polynomial are 3 largest of 11 temperature values recorded at the end of the 60 s ablation period. These three values include the maximum and the two points straddling the maximum. The maximum interpolated temperature is more useful to a physician than just the maximum sensor temperature because it could indicate the abortion of energy delivery quicker when necessary.

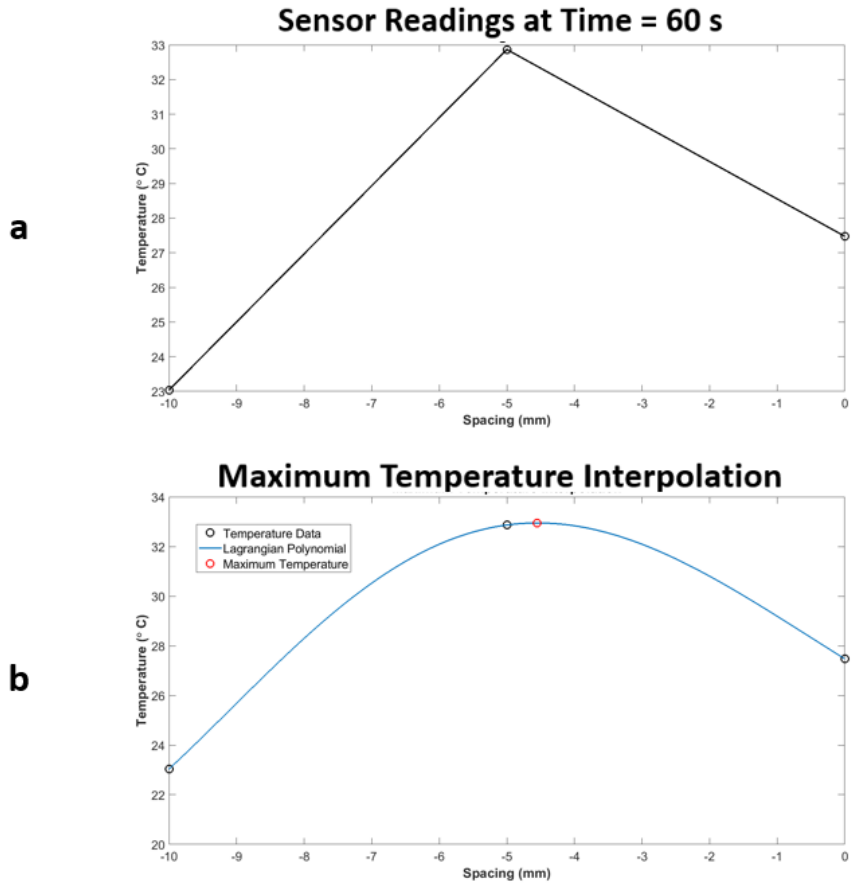

Figure 30: Maximum temperature interpolation between sensors: a) 3 sensor readings from Array #2, b) interpolation between sensors #5 and #6.

3 Thermal Finite Element Analysis

3.1 LS Dyna Heat Transfer Simulation Preprocessing

Thermal finite element analysis (FEA) was used for comparison to experimental results and for adjusting parameters that are difficult to add or change in an ex vivo study. Thermal FEA was employed because the partial differential equations that govern the heat transfer in this problem are very complicated and do not have a closed-form solution. The equation governing the spatial and temporal temperature distribution of heat is shown in Equation 3. This equation can be

augmented to include terms associated with heat loss/gain in the human body. When these terms are included, the equation is also known as the Bio-Heat Equation [29], shown in Equation 4.

$$\boldsymbol{\rho c \frac{\partial T}{\partial t} + \nabla \cdot q + Q = 0} \quad (3)$$

$$\boldsymbol{\rho c \frac{\partial T}{\partial t} + \nabla \cdot q + \rho_b c_b \dot{w}_b (T_{a0} - T) + Q_m + Q_a = 0} \quad (4)$$

The first term of Equation 4 is the temporal term and cannot be ignored because we require a time-dependent solution. The second term accounts for the spatial distribution of heat, where q is the heat flux and ∇ is the del operator. The third term of Equation 4 accounts for heat loss due to perfusion in the heart, where ρ_b, ω_b and c_b are the density, perfusion rate, and heat capacity of blood, respectively. The perfusion term has been shown to be negligible in the results of other computational models for RF ablation and is ignored here for comparison to ex-vivo studies [30]. The fourth term of Equation 4 is the metabolic heat generation and is almost always ignored [31]. It is very small in comparison to the heat generated by the ablative heat source, Q_a, shown by the fifth term. A significant simplification made in this study is to suppress the electrical problem and examine the thermal problem only. Fourier's law, shown in Equation 5, can also be applied here to make the equation in terms of temperature, the dependent variable we want to solve for, rather than the heat flux. With these simplifications, the governing equation is reduced as shown below in Equation 6. The assumed constant term α is the thermal diffusivity (product of heat capacity and density divided by the thermal conductivity).

$$\boldsymbol{q = -k\,\nabla \cdot T} \quad (5)$$

$$\boldsymbol{\alpha \frac{\partial T}{\partial t} - \nabla^2 T + Q_a = 0} \quad (6)$$

It is worth noting that the temperature T and ablative heat source Q_a are functions of space and time. Additionally, this equation must be solved through 2 materials in series. This again shows that there is not an easily obtainable analytical solution for this situation. The FEA package used for the analysis was the commercially available LS Dyna by the Livermore Software Technology Corporation [32].

Figure 9, shown in the 'Ex Vivo Study' section, also helps drive assumptions made in the FEA analysis. Because of the direct contact between the esophagus and the heart, it is assumed that the only mode of heat transfer from the to the esophagus is conduction. A literature review by Berjano et al [31] indicates that convective heat loss can be and is often ignored when studying the local heat transfer associated with cardiac ablation. Another significant assumption for this study is that it can be modeled in two dimensions, in which the sagittal plane is used as the projection. Allowing the assumption of 2 dimensions decreases the computational cost of solving the boundary-value problem and allows more time for adjusting the model and troubleshooting. The two layers of tissue considered are the wall of the left atrium and the wall of the esophagus. Each are assumed to have a uniform thickness of 2.5 millimeters [25]. The transverse length of the tissues in contact is 40 millimeters. The 2D geometry of the simulation in LS Dyna is shown in Figure 31.

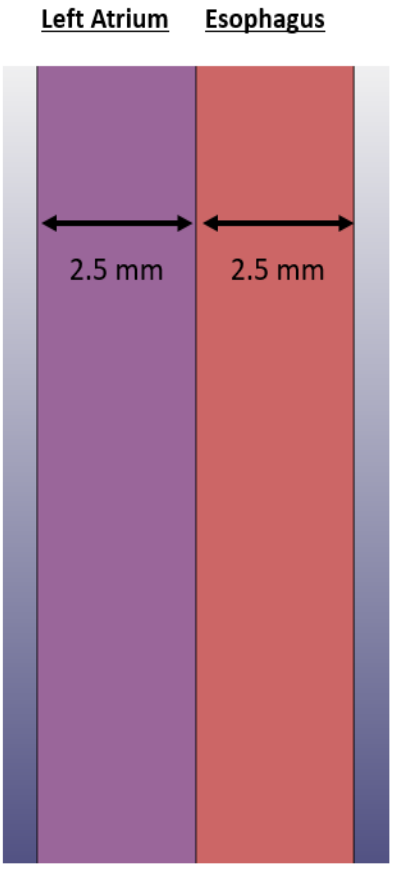

Figure 31: Geometry of FEA study.

The tissue layer geometry was discretized using the '4-N shell' mesh option in LS Dyna. This type of mesh creation prompts the user to define 4 nodes of the geometry/part in space and how the number of elements to be created within the bounds of those nodes. The number of elements created was proportional to the length scales of the geometry so that square elements were created. The thickness of these shell elements in the third coordinate was 1 millimeter. The square shell elements of each part created are shown in Figure 32.

The material model used for the left atrial wall tissue and the esophageal wall tissue was chosen to be thermally isotropic. While real esophageal and left atrial tissue are not necessarily isotropic, this is a good initial assumption when heating occurs through thin layers of material.

The thickness of real tissue varies along the area in contact and may contain additional structures such as glands, epithelia, laminas, nerves, etc. [30]. Table 2 contains the thermal properties used for the two tissues in contact [11].

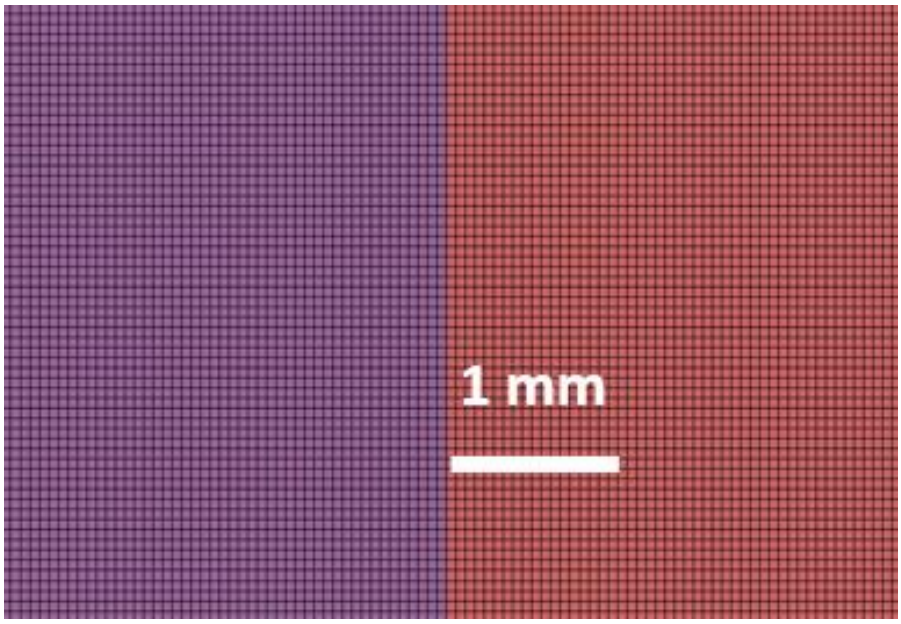

Figure 32: 4-node square shell elements in LS Dyna.

Table 2: Thermal properties applied to the material model in LS Dyna FEA study.

Material	Density $\left(\frac{kg}{m^3}\right)$	Thermal Conductivity $\left(\frac{W}{m * K}\right)$	Specific Heat Capacity $\left(\frac{J}{kg * K}\right)$
Left Atrium	1200	0.7	3200
Esophagus	1000	0.4	3700

A constant-temperature load curve of 55 °C was applied for 60s to a set of nodes that span the medial 5 mm on the of the left atrial tissue geometry, shown in Figure 33, to match the

experimental procedure. The nodes the thermal load is applied to are highlighted in yellow in Figure 34. This removes the irregularities of contact pressure by assuming the catheter is just pressing against the tissue without any force to cause the tissue to elastically deform. The initial temperature of all nodes was room temperature (23 ℃) before the load curve is applied.

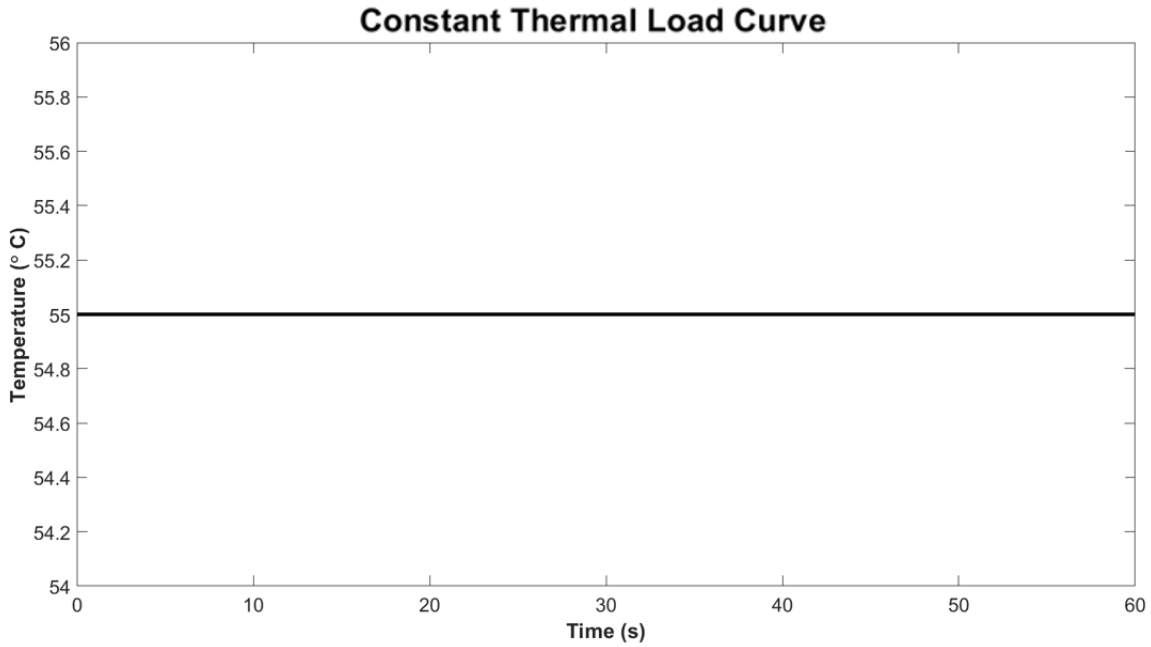

Figure 33: Constant temperature load curve.

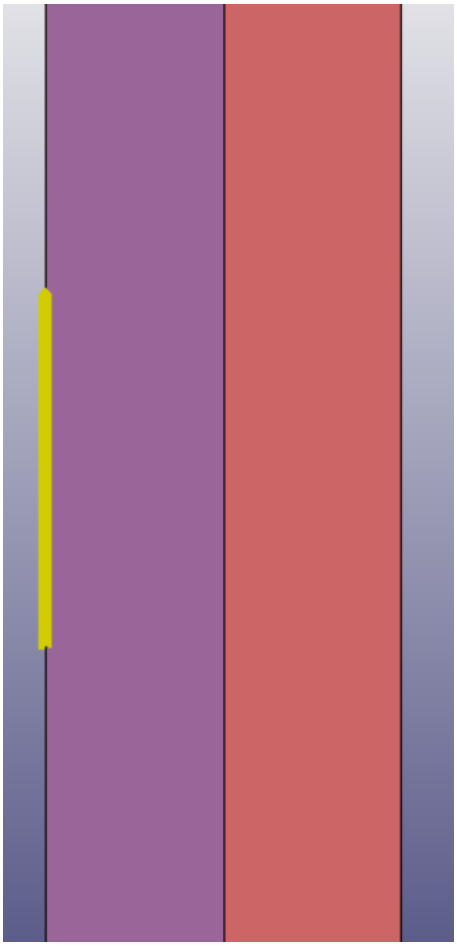

Figure 34: Series of nodes that the temperature load curve was applied to. These nodes span a length of 5 mm and are shown in yellow.

A similar study was also conducted with different loading and initial conditions with the aim to more accurately match realistic catheter ablation. In this study a temperature load curve matching temperature data at the tip of a commercially available ablation catheter [27] was applied to the same set of nodes that span 5 mm in the center of the left atrial tissue. This nonlinear load curve is shown in Figure 35. The initial temperature of all nodes was 37 ℃ to match core body temperature.

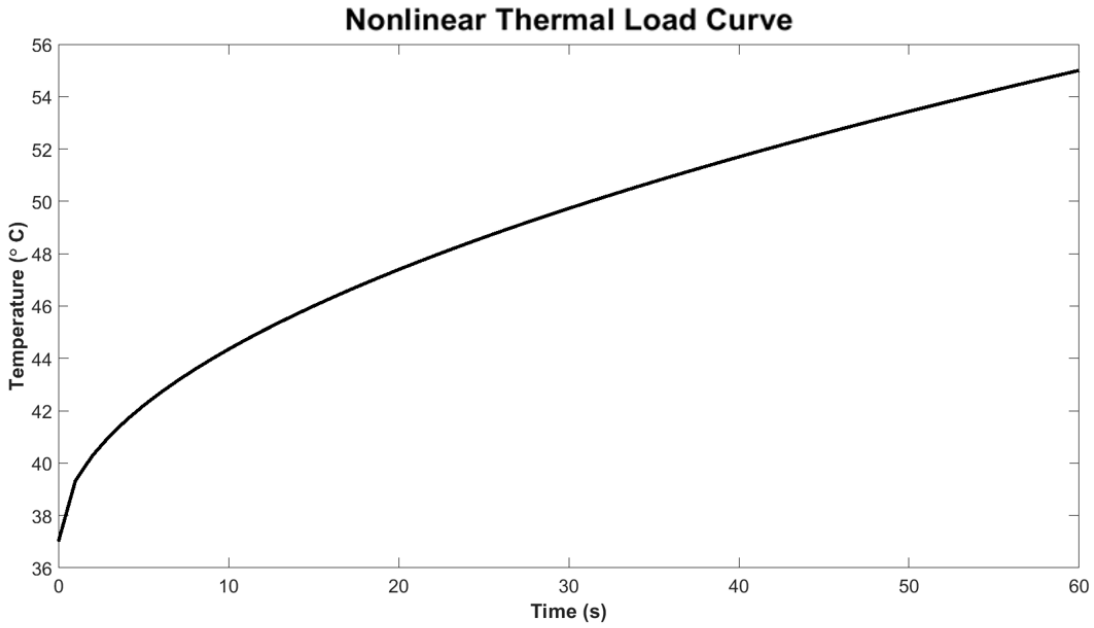

Figure 35: Nonlinear temperature load curve.

Equation 6 above is solved by converting it into Equation 7 (below) in which $[K_T]$, {T}, and {Q} represent the global stiffness/thermal conductivity, global nodal temperatures, and global thermal load matrices, respectively [33]. The global system is made up of individual elemental matrices that correspond to each element of the discretized domain of the problem. This form is created by converting the continuous problem to a discrete problem, often using the Galerkin method [33]. The Galerkin method works by applying variation of parameters to make a weak formulation of the problem which relaxes the conditions of knowing all parameters at all locations and times within the domain. Further, it allows for the problem to be solved within a finite set of basis functions [33].

$$[\boldsymbol{K_T}]\{\boldsymbol{T}\} = \{\boldsymbol{Q}\} \quad (7)$$

The thermal solver chosen for both transient analyses was an iterative diagonal conjugate gradient method. This was the recommended solver by LS Dyna for this application and is often used for large, sparse stiffness matrices [32]. The solver is determined iterative based on the analysis being transient. Node history data was recorded for the entire set of nodes at the endocardium, the luminal esophagus, and the nodes which merge the two parts (layers of tissue) together. Fringe plots of the temperature distribution at the end of the 60s ablation time were also collected. A mesh sensitivity analysis was used to track the trend of maximum temperatures along the history node sets previously mentioned. As the mesh becomes finer, there should be a convergence in the solution to the problem. The number of nodes in each coordinate direction was increased by a factor of 1.5 from each previous simulation. There was a total of six simulations run, and the number of elements corresponding to each is shown in Table 3.

Table 3: Number of elements in each mesh of the simulations used for the mesh sensitivity analysis.

Simulation	Number of Elements
1	80,000
2	180,000
3	320,000
4	720,000
5	1,280,000
6	2,280,000

3.2 FEA Simulation Results

Data from two different FEA studies were collected. The first study, Study #1, matches the conditions in the experimental ex vivo study for validation, i.e., all nodes start at room temperature (23 ℃) and a constant temperature load curve is applied (55 ℃). The second study, Study #2, replicates more realistic operating conditions of catheter ablation in which all nodes start at core body temperature (37 ℃) and experience a temperature load curve shown in Figure 35.

Fringe plots of the temperature distribution in layers of tissue at the end of the 60 s ablation period is shown in Figure 36 and Figure 38. Temperature distribution profiles associated with Study #1 and Study #2 are plotted in Figure 37 and Figure 39, respectively. The node sets used to plot these profiles are the endocardium (where the ablation takes place), the epicardium/outer esophageal wall interface, and the luminal esophageal wall. The flat portion of the endocardium temperature profile is due to the 55 ℃ temperature of the node set in which the load was applied at 60 s.

The maximum temperatures at the outer esophageal wall and luminal esophageal wall at the end of Study #1 were 33.5 ℃ and 26.6 ℃, respectively. The maximum temperatures recorded at the outer esophageal wall and luminal esophageal wall at the end of Study #2 were 40.1 ℃ and 37.6 ℃, respectively.

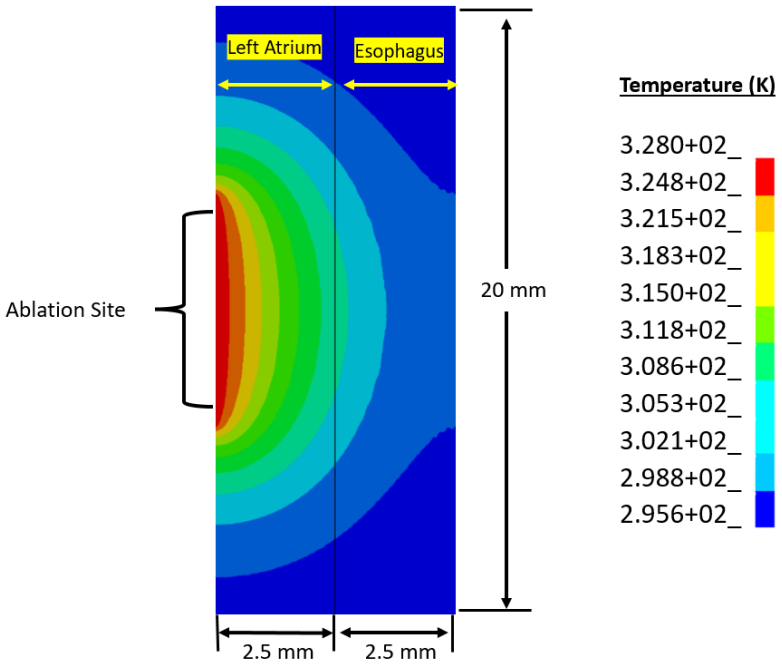

Figure 36: Temperature fringe plot for Study #1 after 60 s ablation in both layers of tissue. The uniform load curve from Figure 32 is used and all nodes were initially set to room temperature.

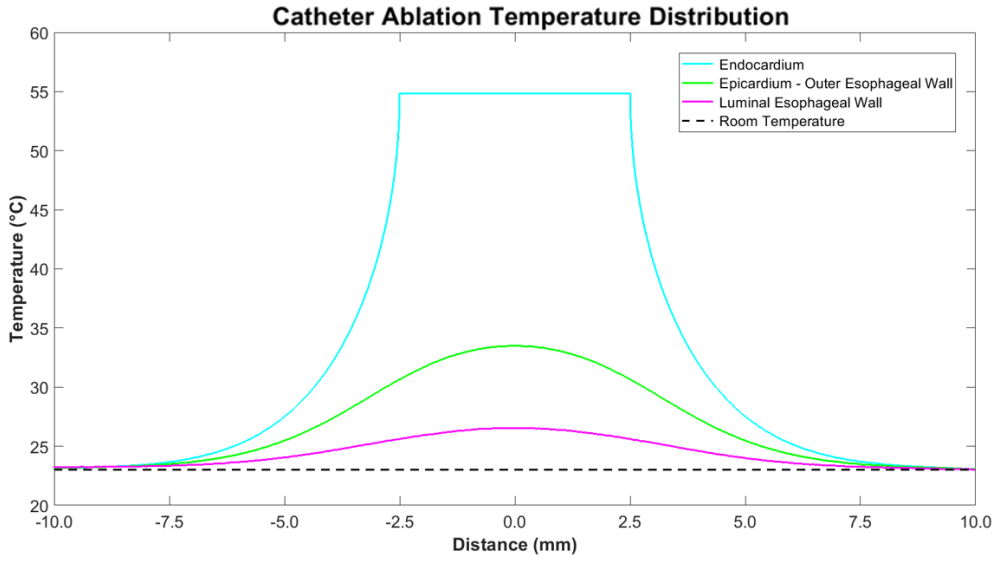

Figure 37: Temperature distribution profiles at three node sets: Endocardium, Epicardium/outer esophageal wall interface, and luminal esophageal wall. The black dotted line indicates room temperature for reference.

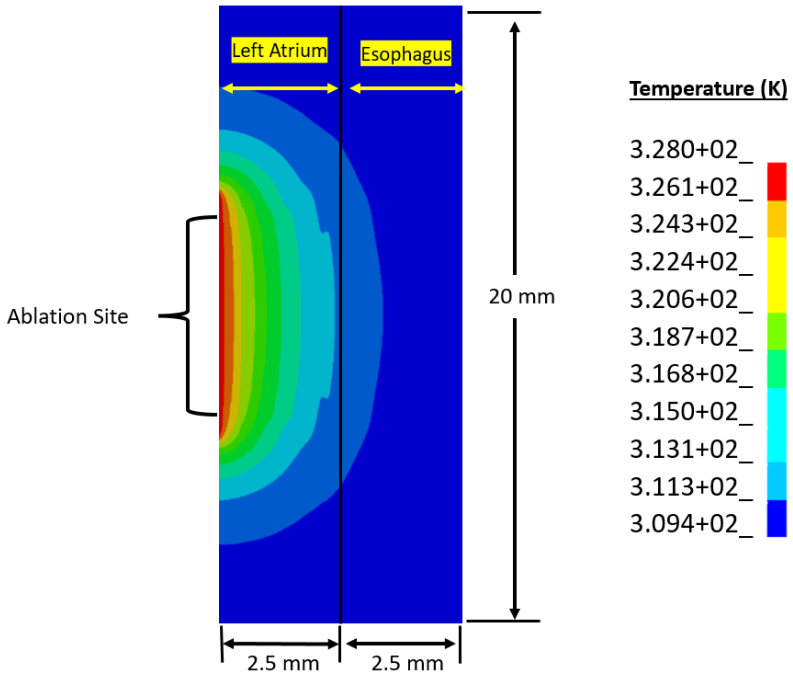

Figure 38: Temperature fringe plot for Study #2 after 60 s ablation in both layers of tissue. The nonlinear load curve from Figure 34 is used and all nodes were initially set to core body temperature.

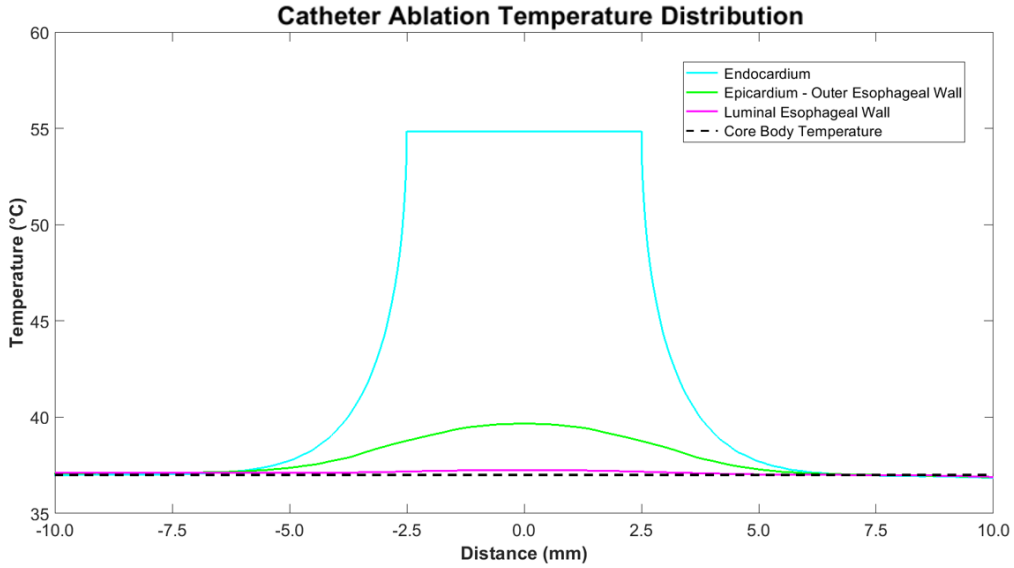

Figure 39: Temperature distribution profiles at three node sets: Endocardium, Epicardium/outer esophageal wall interface, and luminal esophageal wall. The black dotted line indicates core body temperature for reference.

3.3 Discussion of FEA Simulation Results

Thermal FEA results are useful to obtain the temperature distributions at all points of interest. Unlike the experimental results, each node in the FEA simulation acts as a "sensor" that can store the temperature data for all time of the ablation. Since there were many elements used in these simulations, the temperature distribution curves are very smooth and symmetric shown in Figure 37 and Figure 39. These two figures also reveal the actual temperature data that is unable to be seen by colored fringe plots. Ideally, these numerical results from Study #1 match the experimental results with respect to temperature profiles along the luminal esophageal wall. It was found, however, that the simulations do not exactly match the experimental results. For example, maximum temperature at the luminal esophageal wall in the FEA was 26.6 ℃ at 60 s. This is similar the experimental results from ex vivo test B2 in which a maximum temperature of 27.3 ℃ was recorded. Moreover, higher temperatures were recorded in test B1 and test B3.

Figure 40 shows a comparison of the luminal esophageal temperature distribution experimentally (Test B1) and numerically (Study #1). Cubic splines were created between each point to fit the experimental data for sensor #3 - sensor #9. The data was also shifted by 5 millimeters to the right to be centered about zero for comparison. These discrepancies could be due to several factors but is most likely due to tissue thickness variability and extent of contact pressure applied during the experiment. This would also account for the larger spike seen in the polynomial fit and why there is a significant lack of symmetry. As pointed out in Section 2, the maximum temperature of the polynomial through these points is between sensors, not at a single sensor.

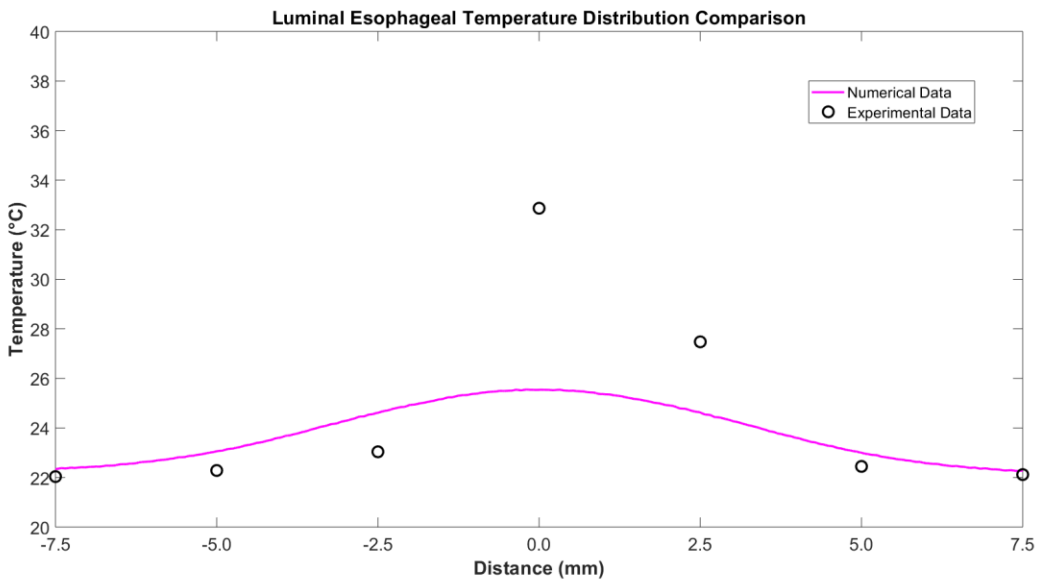

Figure 40: Luminal Esophageal Temperature Distribution Comparison.

The interface temperature profiles for Study #1 vary from those in Study #2 because of the differing initial and loading conditions. As expected, Study #1 shows a larger gradient in temperature between the profiles and baseline temperature (23 ℃) in comparison to Study #2 and its baseline temperature (37 ℃). This is also helps explain the difference in width of the profiles. For example, the temperature profiles in Study #1 are above baseline in a range of 15 millimeters, whereas they are only above baseline in Study #2 for a range of approximately 10 millimeters. The mesh sensitivity analysis shows convergence in the temperature distribution solution. The maximum temperatures at the merged nodes interface and the luminal esophageal nodes are plotted for each simulation in which the number of elements were increased as described in the Methods section above. The percent difference in maximum temperature between the last three simulations were all less than 1%.

As the ex vivo and FEA results are more refined and validate one another, temperature profiles at the endocardium and the epicardium/outer/esophageal interface can be

inferred. This could be important information to give the electrophysiologist, so they may better understand whether they are burning the left atrial tissue enough while knowing the outer wall of the esophagus is safe from thermal injury.

4. Device Prototyping

4.1 Rapid Prototyping Methods

It is always beneficial to prototype an engineered solution to a problem before creating the final product. This is especially true for medical devices in their early development stages, such as the suggested device in this paper. Rapid prototyping efforts utilized here were primarily 3D printing and liquid silicone casting.

Figure 41 shows some of the 3D printing available for creating the prototypes shown in this section. The left image shows the process of fused deposition modeling (FDM) in which material filament is extruded though a heated nozzle layer by layer. The middle image shows a stereolithography apparatus (SLA). In this process, the build plate rises from a pool of resin. A laser within the resin bath translates side to side and applies the laser to cure the resin in the shape corresponding to the stereolithography model it references. The right image shows the process of printing multiple materials with multiple nozzles (commercially known as Polyjet printing). This type of printer sprays layers of photopolymer material out layer by layer [34]. An advantage this type of printing has over other forms of printing is the ability to create parts with variable stiffness.

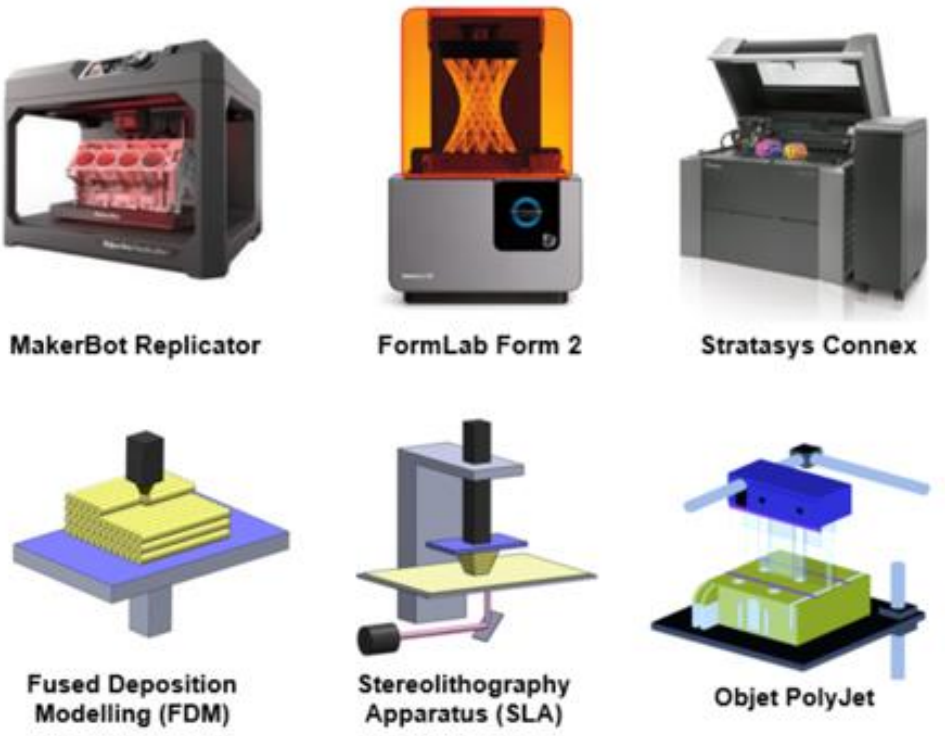

Figure 41: Three different types of printers available for prototyping the luminal esophageal temperature monitoring and esophageal deflection device.

A novel esophageal deflection device is currently in development at the University of California, San Diego (UCSD). Its design is less complex than existing esophageal deviation devices and easier for a physician or nurse to use during the procedure. A 3D printed prototype of the esophageal deflection device (EDD) is shown in Figure 42 using the photopolymer Polyjet method.

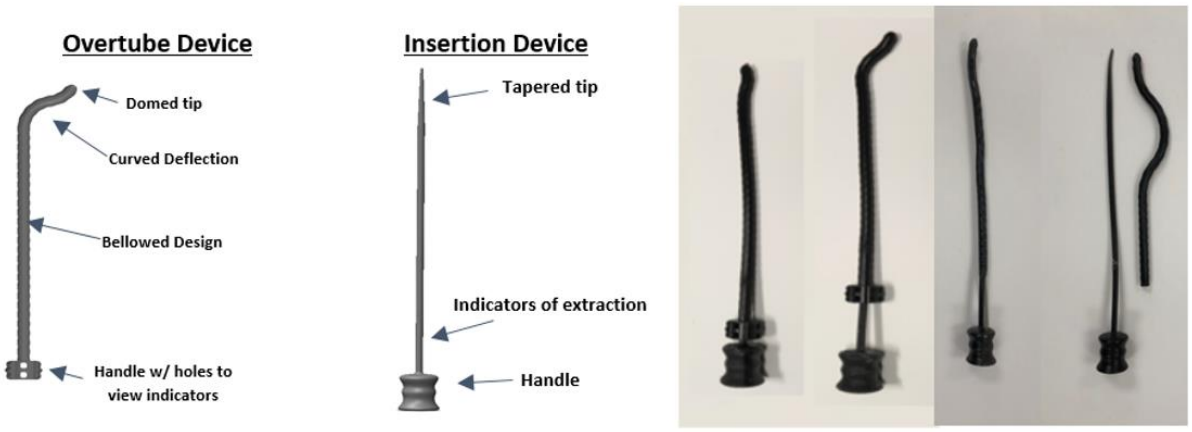

Figure 42: Esophageal Deflection Device (EDD) in development at UC San Diego. Schematic of prototype components (left) and 3D printed prototypes (right). The two 3D printed prototypes show two different deflection states based on overtube design.

The device is made of two main components, an over-tube and an insertion piece. The over-tube is designed and manufactured with a natural curvature and with varying stiffness. The insertion piece is more rigid than the over-tube and can be inserted into the over-tube, thereby straightening the over-tube and eliminating its curvature. When assembled, the device is still flexible enough to maneuver through the mouth and down the esophagus, yet rigid enough to prevent buckling when inserted. After aligning the device, the insertion piece is pulled out of the over-tube, reactivating the curvature of the over-tube and deflecting the esophagus away from the heart. Sufficient torsional stiffness for the over-tube allows for controlled rotation and further maneuvering to ensure the esophagus is diverted away from the ablation site. Unfortunately, the photopolymer material for this printer is not biocompatible and thus there is a need for making the prototype more biocompatible using available resources. 3D printing also makes embedding the sensors along the device more difficult.

Silicone is one the most common material groups used in the fabrication of medical devices, specifically endoscopes and endoscopic-like devices. Many silicones are chemically inert,

biocompatible, sometimes bio-reabsorbable, and can have a unique set of thermal and mechanical properties for specific applications. For rapid fabrication of the luminal esophageal temperature monitoring deflection device, platinum-cure liquid silicone was used for creating the soft biocompatible layer that will be in contact with the luminal esophageal wall.

Commercially available "Smooth On" brand liquid silicone was purchased for the casting procedure. The liquid silicone came in two containers, one of which is cross-linker which, when added to the other in equal parts, begins the curing process. These containers can be seen in Figure 43.

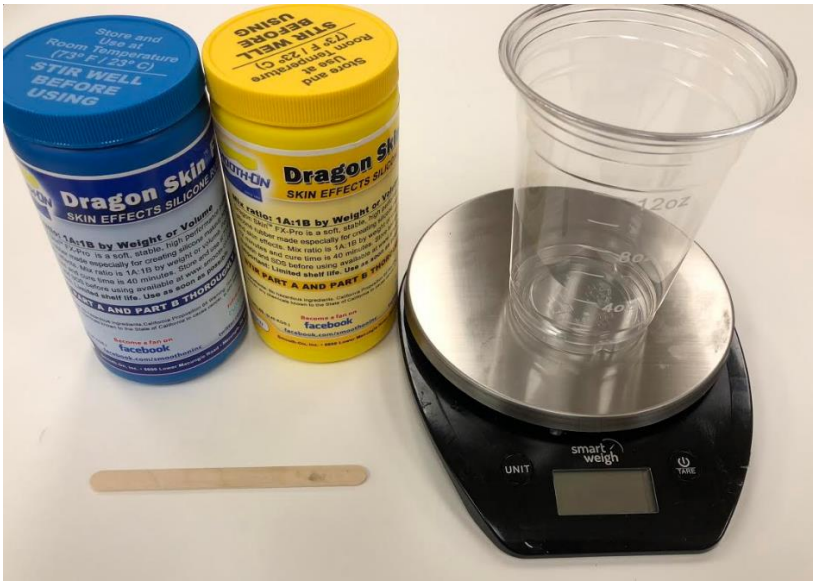

Figure 43: Smooth On brand name liquid silicone containers.

After equal parts of both materials are combined and mixed thoroughly, the mixture is placed inside a vacuum chamber to release the air bubbles that were created during mixing. The degassed mixture is then poured into molds for the device. The cure time listed for the "Dragon Skin – 20" platinum-cure silicone is approximately 4 hours at room temperature. This can vary depending on the actual cure temperature and ratio of the two parts used [35].

4.2 Device Iteration #1

Ideally, sensors within the device are placed in such a way that at least one sensor can capture significant luminal esophageal temperature rises that would indicate a need to remove the heat source. A first iteration prototype of the suggested device is shown in Figure 44. It consists of a rigid support component and multiple thermistors embedded within a hollow, curved tube of silicone. Figure 45 shows the support structure created, made of 2 intersecting coils with a predefined curvature at the distal end. The coils intersect to allow the distal region to be straightened by an insertion piece while impeding bending in the transverse direction. The same thermistors used for the ex vivo study was also used in this prototype. They were placed in orthogonal pairs that alternate their orientation by 90 degrees along the body of the device. This orthogonal pair approach is helpful in situations where ablation is not occurring in the same plane as the sensors. The molds for the silicone casting were also 3D printed with polylactic acid (PLA), shown in Figure 46.

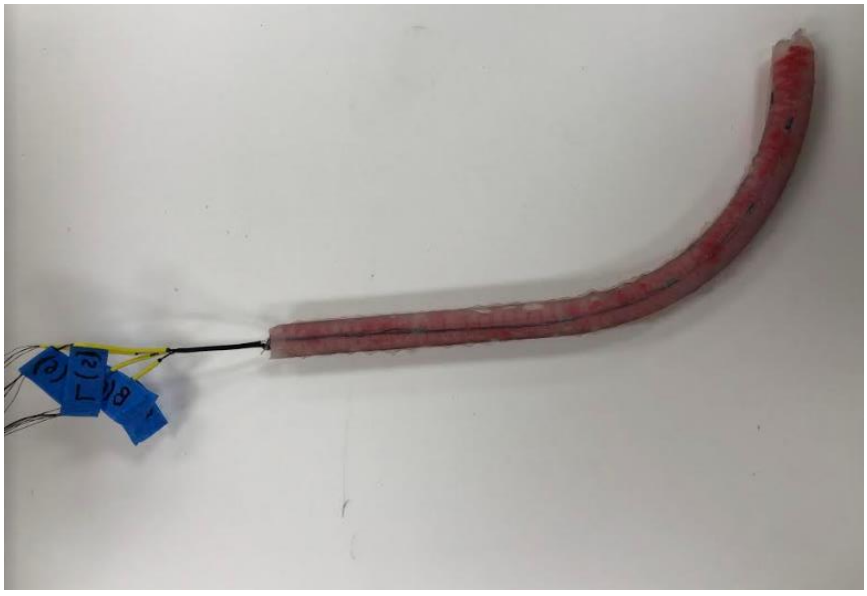

Figure 44: Prototyped device with alternating orthogonal pairs of sensors embedded in a thin hallow tube of silicone.

Figure 45: A 3D printed PLA support structure made of intersecting coils provide additional torsional stiffness for maneuverability after inserted.

Figure 46: Two halves of the mold used to create the liquid silicone casting around the PLA support structure.

4.3 Device Iteration #2

An improved second iteration prototype is shown in Figure 47. This prototype is closer to a biocompatible system and removes the need to 3D print a support structure with predefined curvature.

Figure 47: Prototype using thermoformed commercially available biocompatible tubing.

Instead, the curvature is created by thermoforming a section of commercially available biocompatible thermoplastic elastomer tubing. A series of bolts are fixed into a metal plate to outline the shape of the curvature desired, shown in Figure 48. The curvature is different from the previous prototype in that it is more fully-defined and semicircular in shape. The tubing is placed inside the bolts to keep it in place. Then heat is applied via a heat gun to the entire section of tubing. Afterwards, the tubing is cooled in the same position. This process is repeated until the tubing is set in the desired shape.

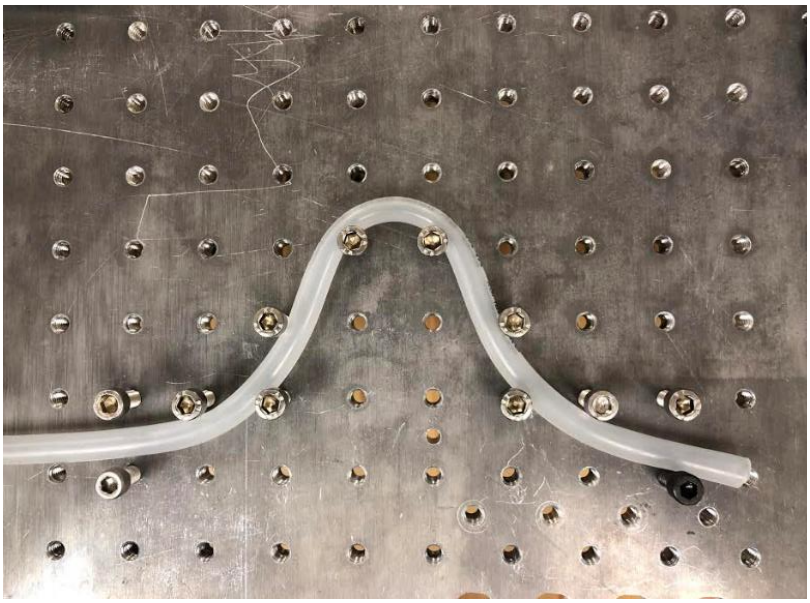

Figure 48: Process for creating the deviation curve in the thermoplastic elastomer tubing.

Thin segments of biocompatible heat shrink were used to keep the thermistors correctly spaced and aligned on the surface of the tubing. The sensors are again put into orthogonal pairs similar to the first iteration, and 5 millimeters apart, based on results from the ex vivo and FEA results. The three strips on the device in Figure 47 are used to show where radiopaque markers may be put in the device. These markers show the upper and lower bounds of the thermistor array, as well as the center point between the two limits, which is also the point of maximum deflection from the straightened section when the insertion piece is removed. The prototype inside its mold during the silicone curing process is shown in Figure 49.

The problem of inadequate contact between the sensors and the luminal esophageal wall was solved using suction. The hallow lumen of the outer tube and insertion piece are capable of sucking air out of the esophagus so that the esophagus would conform around the shape of the device. The outer diameter of the device is approximately 12 millimeters, below the average inner

diameter of the esophagus [36]. This enables the sensors to be in contact with the esophageal wall, even when the device is activated to deflect.

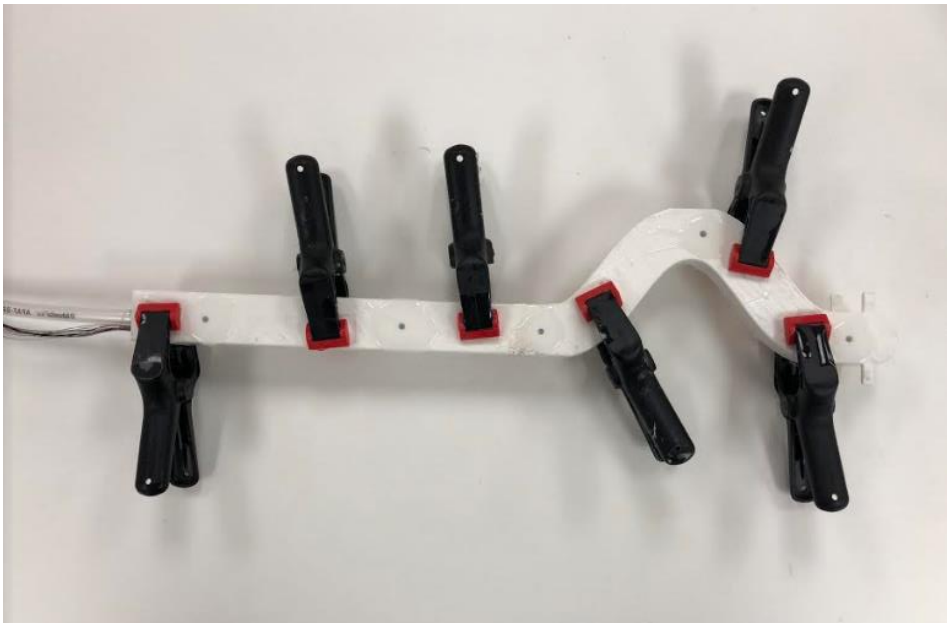

Figure 49: Clamped molds used during silicone curing process around the tubing with attached thermistors.

5. Commercialization

The regulatory pathway will depend on the features of the device, as well as its indications for use. One potential pathway is for the device to be regulated under an existing Class I product code. This would limit its function to deflect the esophagus only. If the device is determined to be 510(k) exempt, the device may be marketed without FDA approval. This would not require human clinical trials (animal testing only). The EsoSure esophageal deflector is an example of an exempt device that performs similarly to this technology and is considered a “retractor” by the FDA.

Since the proposed device will be capable of temperature monitoring, it is considered electrical medical equipment because it will have wired sensors. The device would most likely be a Class II device and would minimally require a 510(k) pre-market notification [37]. The 510(k)

is only a minimum requirement if there is a predicate device that is shown to be substantially equivalent to a legally marketed device.

Because there is currently no device that incorporates both deflection and temperature monitoring, the FDA may consider this device to be novel and require a de novo submission and human clinical trials before FDA clearance. The FDA does however allow for a "split-predicate" device where the primary predicate has the same intended use and the indications for use as the proposed device, along with a "reference predicate", which supports equivalence of the technology. Thus, it may be possible that the FDA would allow the Class II device to be cleared as a clinical temperature probe and the 510(k) would be a possibility. The FDA also maintains a process to request feedback on device classification as described in section 513(g) of the Federal, Drug, and Cosmetic Act [37]. This provides means for understanding the agency's views about the regulation and requirements that may be applicable to a new device.

To date, there are no consistent coding schemes that describe the placement/use of the proposed device, no specific guidance in medical coverage policy, and no payment mechanisms for a physician who would place the device. This is a classic example of the reimbursement challenges faced by many who develop novel medical devices. Consequently, the device would require development of a Category I or Category III current procedural terminology (CPT) code if a physician's use is to be separately coded and charged [37]. Otherwise, placement of the device would be considered an incidental service which would still be covered but not separately paid to the physician [37]. For many "me too" devices, in hospitals, "pass-through" codes may be used. This assists with billing cost including a markup determined by a hospital and this is the case for most devices used in an electrophysiology lab. The costs assigned would then be passed onto the patient's insurance.

It has been determined that the proposed device is likely to be used by the electrophysiologist and not a nurse or anesthesiologist. This is primarily because insertion of the device requires an additional set of skills, exposes such individuals to potential malpractice, and would not necessarily be used in all cardiac ablation procedures. This information insinuates that there is a need for creating a new CPT code and associated relative value unit (RVU) development. This also includes creating a new code for hospital billing and a publication strategy for accumulating sufficient peer-reviewed articles to demonstrate the clinical value and appropriateness for coverage [37].

Ultimately, it would be the institutions (primarily hospitals) that would purchase the device [37]. They would not see any direct payment for use of the device in the institution. Alternatively, they would benefit via adjusted DRG and APC weights to help recapture cost of purchasing. These weights would be adjusted after the institutions can prove that they have safer cardiac ablation procedures with fewer complications and better outcomes (particularly with respect to esophageal damage). If the FDA would clear such a device, an unlisted CPT code could be used by professional and institutional providers as an interim step for billing until a new CPT code is created.

6. Conclusion and Future Scope

When developing solutions to one problem, new problems are sometimes created. In this case, catheter ablation presents the problem of potentially damaging the esophagus due to the local heat transfer though the left atrium. Even though the ablation procedure is what causes thermal injury, it is one of the best treatment options for atrial fibrillation and will be continued to be used despite potential complications that arise. The positive impact outweighs the negative impact.

Thus, there is a definitive need to create and improve upon devices that solve the complications involved.

In this paper, the preliminary development of a novel esophageal deflection and improved temperature sensing/monitoring device is described. The device is intended to be used in all catheter ablation procedures to ensure the safety of the patient during the procedure. A primary goal was to better understand the heat transfer to the esophagus from an ablation catheter. This understanding helps guide the placement and spacing of the sensors to ensure that any dangerous temperature increase to the esophagus is detected by the electrophysiologist or medical staff performing the ablation.

Mimicking the ablation procedure was done in two ways. The first was an ex vivo study in which excised porcine heart and esophageal tissue was subjected to a catheter-like heat source. Temperature sensor arrays show the heat distribution to the luminal esophageal wall. It was shown that a relatively small spacing of temperature sensors is necessary for adequately recording dangerous temperature rise. FEA models also show how this temperature distribution develops over time. As predicted, it was shown that decreasing the distance between sensors on the device increases the chance of detecting temperature changes in the esophagus. Although decreasing this distance is effective, there needs to be additional work with respect to the selection of biocompatible materials that acts as the barrier between the sensors and the esophageal wall. Figure 50 shows the setup for more tests that will take place in the future.

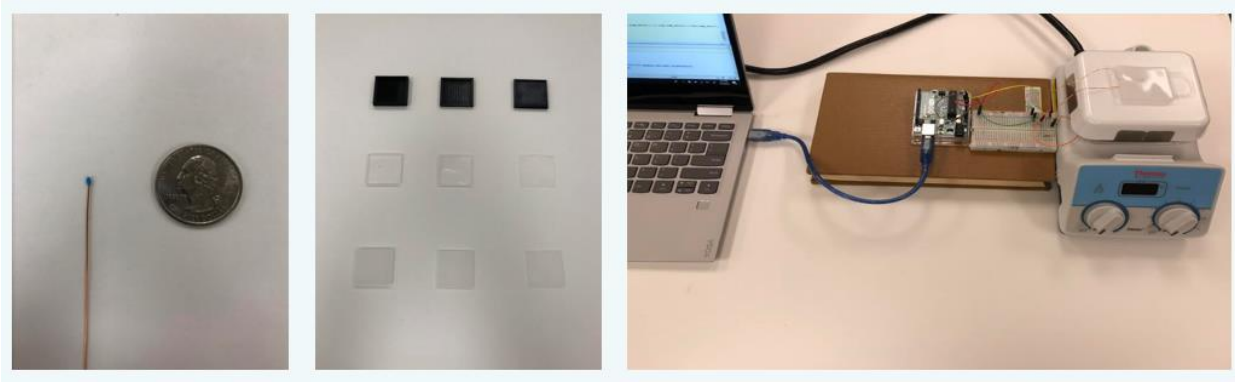

Figure 50: Setup for future tests that investigate temperature sensor response time through layers of biocompatible material.

In this study, a heat source (hot plate) is applied to the sensors through layers of silicone with varying thickness. This will help determine an acceptable thickness needed to sense a quick response to an applied heat source. Additional work is also needed for finding the optimal sensors to use for this application. There are other types of sensors and other commercially available brands of thermistors that may be better candidates. These types of tests will help produce improved prototypes which will move the device closer to a final design.

Future work in ex vivo studies will be to use a real ablation catheter and RF generator that can be used to better mimic the ablation process. While the constant temperature heat source used is a satisfactory tool for initially replicating the heat generated at the epicardium, the temperature load is different due to the nature of energy delivery in a real catheter. Another improvement in these studies is to perform the tests at core body temperature. The tests described above were at room temperature and do not reflect the actual temperature gradients between the catheter and layers of tissue.

Future work in thermal FEA is to first couple the thermal problem with the electrical problem, as done by Perez et al [24] to study the RF antennae effect of ETPs during ablation. Material models will also need improvement to account for the non-thermal isotropic behavior of

the tissues in contact. Better material properties for the left atrial and esophageal tissue will be investigated to increase accuracy. Contact pressure measurements will also be implemented, as this is shown to be a significant variable to take into consideration. In fact, there has been a trend in the ablation catheter market to include pressure sensors to show the physician how much force they are applying in the left atrium. In 2014, there was an approximate 60% increase in contact pressure-sensing ablation catheters [10]. Also, between 2014-2016, approximately 50% of the market moved from non-pressure-sensing to pressure-sensing catheters [10]. Convective cooling due to irrigation techniques and heat loss due to perfusion of blood pumping through the heart should also be considered. Finally, the FEA model could benefit from an accurate 3D representation of the organ structures and heat source, rather than the 2D representation used here.

The reimbursement and regulatory options for this device is difficult, mostly because it will most likely be considered novel electrical medical equipment. Therefore, a De Novo submission will likely be required unless there are substantial predicate devices that can warrant a 510(k)-pre-market notification. A deeper understanding of the exact indications of use and who will be operating the device will be keys to developing the reimbursement structure. As the overall world population ages and the amount of catheter ablation procedures increases, there is great confidence that this device will help save lives once fully developed and placed in the hands of physicians.

References

[1] H. Calkins, Jais Pierre, and J. S. Steinberg, A Practical Guide to Catheter Ablation of Atrial Fibrillation, vol. 2. Philadelphia: Wolters Kluwer – Lippincott Williams & Wilkins, 2015.

[2] "Atrial Fibrillation," How Cigarettes Damage Your Body. [Online]. Available: http://www.heart.org/en/health-topics/atrial-fibrillation.

[3] Luqman, "Diagram Of A Human Heart Human Heart Diagram Without Labeling Human Heart Diagram With," Human Anatomy Diagrams, 18-Dec-2017. [Online]. Available: https://anatomyclass01.us/diagram-of-a-human-heart/diagram-of-a-human-heart-human-heart-diagram-without-labeling-human-heart-diagram-with/.

[4] "Treatment of AFib: Is Ablation That Good or is Drug Therapy That Bad?," American College of Cardiology. [Online]. Available: https://www.acc.org/latest-in-cardiology/articles/2014/07/18/15/17/treatment-of-afib-is-ablation-that-good-or-is-drug-therapy-that-bad.

[5] N. Muselimyan, L. M. Swift, H. Asfour, T. Chahbazian, R. Mazhari, M. A. Mercader, and N. A. Sarvazyan, "Seeing the Invisible: Revealing Atrial Ablation Lesions Using Hyperspectral Imaging Approach," Plos One, vol. 11, no. 12, Aug. 2016.

[6] V. Y. Reddy, P. Neuzil, S. Themistoclakis, S. B. Danik, A. Bonso, A. Rossillo, A. Raviele, R. Schweikert, S. Ernst, K.-H. Kuck, and A. Natale, "Visually-Guided Balloon Catheter Ablation of Atrial Fibrillation: Experimental Feasibility and First-in-Human Multicenter Clinical Outcome," Circulation, vol. 120, no. 1, pp. 12–20, 2009.

[7] "Atrial fibrillation Ablation," Mayo Clinic, 24-Mar-2018. [Online]. Available: https://www.mayoclinic.org/tests-procedures/atrial-fibrillation-ablation/about/pac-20384969.

[8] "Search Our Products," Biosense Webster, Inc. - A History of Innovation. [Online]. Available: https://www.biosensewebster.com/. [Accessed: 13-Aug-2018].

[9] W. S. Tzou and A. M. Russo, "Luminal Esophageal Temperature Monitoring for the Prevention of Esophageal Injury During Left Atrial Ablation: LET" Journal of Cardiovascular Electrophysiology, vol. 24, no. 9, pp. 965–967, 2013.

[10] "St. Jude Medical 2016 Investor Conference," in Annual Investor Conference, 2016.

[11] A. Fasano, L. Anfuso, S. Bozzi, and C. Pandozi, "Safety And Necessity Of Thermal Esophageal Probes During Radiofrequency Ablation For The Treatment Of Atrial Fibrillation," Journal of Atrial Fibrillation, vol. 9, no. 1, 2016.

[12] J. C. P. Mateos, E. I. P. M, T. G. S. Peña, T. J. Lobo, J. C. P. Mateos, R. N. A. Vargas, C. T. C. Pachón, and J. C. Z. Acosta, "Simplified Method for Esophagus Protection during Atrial Fibrillation Radiofrequency Catheter Ablation - Prospective Study of 704 Cases," Revista Brasileira de Cirurgia Cardiovascular, 2015.

[13] G. Feld, "UCCAI Interview: Dr. Gregory Feld.".

[14] "Heart Pictures, Diagram & Anatomy | Body Maps," Healthline. [Online]. Available: https://www.healthline.com/human-body-maps/heart.

[15] M. Dewhirst, B. L. Viglianti, M. Lora-Michiels, P. J. Hoopes, and M. A. Hanson, "Thermal dose requirement for tissue effect: experimental and clinical findings," Thermal Treatment of Tissue: Energy Delivery and Assessment II, Feb. 2003.

[16] C. Pappone, G. Vicedomini, and V. Santinilli, "Atrio-Esophageal Fistula After AF Ablation: Pathophysiology, Prevention &Treatment," Journal of Atrial Fibrillation, vol. 6, no. 3, Oct. 2013.

[17] K. Koranne, I. Basu-Ray, V. Parikh, M. Pollet, S. Wang, N. Mathuria, D. Lakkireddy, and J. Cheng, "Esophageal Temperature Monitoring During Radiofrequency Ablation of Atrial Fibrillation: A Meta-Analysis," Journal of Atrial Fibrillation, vol. 9, no. 4, 2016.

[18] Perzanowski C, Teplitsky L, Hranitzky PM, Bahnson TD. Real-time monitoring of luminal esophageal during left atrial radiofrequency catheter ablation for Koranne et al 15 atrial fbrillation: observations about esophageal heating during ablation at the pulmonary vein ostia and posterior left atrium. J. Cardiovasc. Electrophysiol. 2006; 17: 166-70.

[19] "CIRCA's S-CATH™ Hot & Cold Esophageal Temperature Monitoring System – CIRCA's S-CATH™ Hot & Cold Esophageal Temperature Monitoring System," CIRCAs SCATH Hot Cold Esophageal Temperature Monitoring System. [Online]. Available: http://www.circascientific.com/.

[20] "St. Jude Medical Sensitherm," St. Jude Medical. [Online]. Available: https://www.sjmglobal.com/professionals/resources-and-reimbursement/technical-resources/electrophysiology/recording-monitoring/monitoring-systems/sensitherm-esophageal-temperature-monitoring-system?halert=show&clset=92f57278-460e-4300-b7fe-89e52a04194f%3acadddb93-fcc4-47f2-8ceb-fd88f01ca17f

[21] "EsoSure - Safely moves the esophagus," EsoSure - Safely moves the esophagus. [Online]. Available: https://www.esosure.com/.

[22] http://www.manualsurgicalsciences.com/products.html.

[23] L. R. Leite, S. N. Santos, H. Maia, B. D. Henz, F. Giuseppin, A. Oliverira, A. R. Zanatta, A. K. Peres, C. Novakoski, J. R. Barreto, F. Vassalo, A. Davila, and S. M. Singh, "Luminal Esophageal Temperature Monitoring With a Deflectable Esophageal Temperature Probe and Intracardiac Echocardiography May Reduce Esophageal Injury During Atrial Fibrillation Ablation Procedures: Results of a Pilot Study," Circulation: Arrhythmia and Electrophysiology, vol. 4, no. 2, pp. 149–156, 2011.

[24] J. J. Pérez, A. Davila, A. Aryana, and E. Berjano, "Electrical and Thermal Effects of Esophageal Temperature Probes on Radiofrequency Catheter Ablation of Atrial Fibrillation: Results from a Computational Modeling Study," Journal of Cardiovascular Electrophysiology, vol. 26, no. 5, pp. 556–564, 2015.

[25] D. Quintana, "Anatomic Relations Between the Esophagus and Left Atrium and Relevance for Ablation of Atrial Fibrillation," Circulation, vol. 112, no. 10, pp. 1400–1405, Jun. 2005.

[26] C. Seo, D. Stephens, J. Cannata, A. Dentinger, F. Lin, S. Park, D. Wildes, K. Thomenius, P. Chen, T. Nguyen, A. Delarma, J. Jeong, A. Mahajan, K. Shivkumar, O. Oralkan, P. Khuri-Yakub, and M. O'Donnell, "Monitoring Radiofrequency Catheter Ablation using Thermal Strain Imaging," 2011.

[27] D. N. Stephens, J. Cannata, R. Liu, J. Z. Zhao, K. K. Shung, H. Nguyen, R. Chia, A. Dentinger, D. Wildes, K. E. Thomenius, A. Mahajan, K. Shivkumar, K. Kim, M. O'Donnell, A. Nikoozadeh, O. Oralkan, P. T. Khuri-Yakub, and D. J. Sahn, "Multifunctional Catheters Combining Intracardiac Ultrasound Imaging and Electrophysiology Sensing," IEEE Trans. Ultrason., Ferroelect., Freq. Contr., vol. 55, pp. 1570–1581, 2008.

[28] "Temperature coefficient," Wikipedia, 27-Jul-2018. [Online]. Available: https://en.wikipedia.org/wiki/Temperature_coefficient.

[29] W. Yang, T. C. Fung, K. S. Chian, and C. K. Chong, "Directional, Regional, and Layer Variations of Mechanical Properties of Esophageal Tissue and its Interpretation Using a Structure-Based Constitutive Model," Journal of Biomechanical Engineering, vol. 128, no. 3, p. 409, 2006.

[30] A. Lakhssassi, E. Kengne, and H. Semmaoui, "Modifed pennes equation modelling bio-heat transfer in living tissues: analytical and numerical analysis," Natural Science, vol. 02, no. 12, pp. 1375–1385, 2010.

[31] E. Berjano, "Theoretical modeling for radiofrequency ablation: state-of-the-art and challenges for the future." 2006.

[32] "LS-DYNA," LS-DYNA | Livermore Software Technology Corp. [Online]. Available: http://www.lstc.com/products/ls-dyna.

[33] D. L. Logan, A first course in the finite element method. Australia: Cengage Learning, 2017.

[34] “What is PolyJet Technology?,” Connex3 – Rapid Tooling und Rapid Prototyping mit mehreren Materialien | Stratasys. [Online]. Available: http://www.stratasys.com/polyjet-technology.

[35] “Dragon Skin® 20 Product Information,” Smooth-On, Inc. [Online]. Available: https://www.smooth-on.com/products/dragon-skin-20/.

[36] R. K. Goyal, P. Biancani, A. Phillips, and H. M. Spiro, “Mechanical properties of the esophageal wall,” Journal of Clinical Investigation, vol. 50, no. 7, pp. 1456–1465, Jan. 1971.

[37] “Esophageal Deflection Device Regulatory and Reimbursement Strategy,” rep.